Molecular Properties from Combined QM/MM Methods. 2. Chemical Shifts in Large Molecules

Qiang Cui and Martin Karplus*

Department of Chemistry and Chemical Biology, Harvard University, 12 Oxford Street, Cambridge, Massachusetts 02138, and Laboratoire de Chimie Biophysique, Institut Le Bel, Université Loius Pasteur, F-6700 Strasbourg, France

Received: November 23, 1999; In Final Form: January 13, 2000

A method for calculating the chemical shielding tensor of any atom with the QM/MM approach has been developed. The method is described and applied to a number of model systems including the water dimer, NMA−water complexes, cytosine monophosphate, paired and stacked nucleic acid bases, imidazole−metal complexes, and 1′-deoxyribose−metal ion complexes. The results demonstrate that with an appropriate QM/MM partition, good descriptions of the environmental effects on chemical shift tensors are obtained. The typical error compared to full QM calculations is 1−2 ppm for heavy atoms. At distances below 2.5 Å, such as occur in hydrogen bonding, larger errors arise due to the lack of Pauli repulsion and magnetic susceptibility of the nearby groups in the current QM/MM model; including the hydrogen bonded molecules as part of the QM region is a way of solving this problem. The method is also applied to a simple model of myoglobin−CO and it is shown that the significant influence from the distal histidine on the shielding of Fe and CO is well reproduced by a QM/MM calculation. Application to the chemical shift of the 1-N nitrogen in nicotinamide adenine dinucleotide (NAD^+), relative to *N*-methyl nicotinamide, gives good results, indicating that accurate chemical shifts can be obtained for specific atoms in large molecules that cannot be treated by QM at the MP2 level. The effect of solvation on the chemical shift of water was also studied with the QM/MM approach in a molecular dynamics framework. The test calculations described in this paper demonstrate that the QM/MM method for estimating shielding tensors and chemical shifts is a useful approach for large systems.

I. Introduction

Nuclear magnetic resonance (NMR) is a widely used tool for studying the structure and dynamics of chemical and biological systems ranging from small molecules to proteins and nucleic acids.[1] Many measurable parameters are of interest, including chemical shifts, spin−spin coupling constants, the nuclear Overhauser effect (NOE), and relaxation times. Although chemical shifts are determined and assigned in an essential step of any NMR study, it has been shown only recently that they can provide useful information for protein structure determination.[2] In some cases, chemical shift constraints have been found to be essential for the refinement of protein structures.[3] The theory of chemical shielding was developed many years ago,[4] and calculations of chemical shielding tensors for diatomic molecules were made in the early 1960s,[5] but only in the past decade have *ab initio* methods and density functional theories (DFT) been used for the prediction of chemical shielding for larger systems.[6] A new implementation of the gauge including atomic orbital (GIAO) method[7] makes it more efficient and directly competitive with the individual gauge for localized orbitals (IGLO)[8] and localized orbitals/localized origins (LORG) approaches,[9] which are not easily extended to correlated wave functions. For small molecules containing up to 10 heavy atoms,[10] high-accuracy calculations based on MP2[11] and CCSD(T)[12] *ab initio* theories have been made within the GIAO framework. Since DFT is the most useful quantum mechanical technique for larger systems,[13] particularly where metal ions are involved, implementations for calculating magnetic properties such as chemical shielding tensors within the DFT framework are of considerable importance. The Hohenberg−Kohn variational principle requires extension in the presence of a magnetic field because the exchange-correlation density functional depends on both the electronic density and the paramagnetic current density.[14] Use of such a functional is the basis of the current-density functional theory (CDFT).[15,16] However, in most implementations, the standard exchange-correlation functionals, independent of the current density, are used. This is justified, in part, by the work of Handy et al.,[16] who found that the effect on the computed chemical shielding from the paramagnetic current in the exchange-correlation functional is rather small. With DFT, it is possible to treat systems of up to about 100 atoms, and the results are generally in good agreement with experiment. The errors are in the range of 10 ppm for ^{13}C and 20 ppm for ^{15}N for the isotropic component of the shielding tensors.[17] The errors are reduced by about a factor of 2 at the MP2 level[11] in calculations for small molecules.[17] Implementation of the sum-over-states density functional perturbation theory (SOS-DFPT) with IGLO choice of gauge origins by Malkin and co-workers has also given good results.[6,18] The good agreement between SOS-DFPT and experiment has been rationalized in terms of the use of improved Kohn−Sham eigenvalues, which are introduced by a somewhat *ad hoc* procedure.[16] The effect of spin−orbit coupling on the chemical shielding in systems containing heavy elements has also been studied.[19] Applications include organic molecules such as unusual carbon cations,[20] organometallic compounds,[21] and zeolites,[22] as well as models

10.1021/jp994154g CCC: $19.00
Published on Web 03/18/2000

for interactions in proteins.[23] These results illustrate the power of computations in providing guidance for experimental spectral assignment and in improving our understanding of the factors that affect the chemical shielding tensor.

For macromolecules, including proteins[24] and nucleic acids,[25] useful empirical and semiempirical methods for chemical shift estimates have been developed. They are based on measured values for different systems, augmented by semiempirical calculations. The recent increase in the number of protein structures determined by NMR has made possible a simple, yet useful, empirical description for proton chemical shifts. The model includes electric field effects, the contribution of the magnetic susceptibility of other atoms or groups, and close-contact interactions.[26] The electrostatic effect is usually treated with the Buckingham formula,[27] which works well for proton chemical shifts, but little has been done for ^{13}C and ^{15}N,[28] especially for chemical shift anisotropies. The magnetic susceptibility contribution, mainly from carbonyl groups and aromatic rings, is usually treated in the magnetic dipole approximation with the McConnell equation.[29] The close contact term has been modeled by use of the Drude model for dispersion.[30] Although it is now recognized that the close contact term originates mainly from the Pauli repulsion, rather than from dispersion,[2d,31] the Drude form is kept in most applications since the two effects have a similar distance dependence and the parameters involved are obtained by a fitting procedure. Such empirical approaches have been demonstrated to be useful in protein structural refinement.[3]

To complement these empirical approaches and to treat nuclei other than the proton, it is important to be able to calculate chemical shielding with high accuracy for specific groups in a large molecule. This requires a method that treats the shielding of only part of the system in detail and describes the environment by a simpler and fast approach. QM/MM methodologies[32] are well suited for this purpose. Recently, we have developed and implemented vibrational calculations in the QM/MM framework with the QM part treated by Hartree−Fock or DFT, and the MM part treated with an empirical (CHARMM) force field.[33] Analytical methods for calculating the Hessian matrix and infrared intensities were described. It was shown for model systems (including formamide in water, a model transition state structure of triosephosphate isomerase and a simple active site model for CO binding to myoglobin) that satisfactory results can be obtained for the effect of the environment treated by MM, as compared with full *ab initio* calculations. In the current work, we extend the QM/MM method to the calculation of the chemical shielding tensor. We describe the method, its implementation in Gaussian 98,[34] and illustrate it by a number of applications, including the water dimer, *N*-methylacetamide (NMA)−water, cytosine monophosphate, base pairing and stacking, imidazole, 1′-deoxyribose−metal ion systems, and an active site model of myoglobin−CO plus the example of NAD^+. We have chosen the Gaussian program for the present development because it has an efficient implementation of the GIAO approach at various QM levels, including Hartree−Fock, DFT, and MP2. Implementation of the QM/MM methodology with other QM and MM programs should be straightforward.

A number of related studies have appeared. de Dios et al.[35] have considered the electrostatic effect of the environment represented by partial atomic charges or electric field gradients. Good results were obtained for small model systems, and computed chemical shift results were found to be useful in relating the observed chemical shifts to the secondary structure for a number of proteins. For valine sidechains, it was observed that the calculated chemical shifts were in only qualitative agreement with experiment if the X-ray structure was used. Improved results were obtained when sidechain conformations were optimized with either *ab initio* quantum chemical or empirical methods, suggesting that the crystal orientations were not the correct conformers in solutions; DFT gave better values than HF for the shielding tensors.[36] Brüschweiler et al.[37] have recently used the SOS-DFT approach to analyze the effect of the environment on ^{15}N chemical shift anisotropy (CSA) of two Gln residues in ubiquitin. The environment was modeled by partial charges, and the coordinate sets were obtained from molecular dynamics simulations. It was found that the effect on CSA could be significant; the range of values was on the order of 16 ppm, relative to −144 ppm. In the active sites of zeolites, Truong and co-workers[6a,38] have used point charges to mimic the Madlung potential; they calculated chemical shift of absorbed NH_3 in good agreement with experiment. Approaches for calculating chemical shielding with the polarizable continuum model (PCM) have been reported by Cremer et al.[39] and Tomasi et al.[40]

The present treatment is a general approach to chemical shielding calculations within the QM/MM framework. It is part of the CHARMM program that can be used for minimizing a structure or doing molecular dynamics. In this way, it becomes possible to relate the predicted shielding to the structure and to determine the contribution of the chemical shielding anisotropy to spin relaxation, for example.[41] Although much attention has been paid on the *overall* correlation of protein secondary or tertiary structure and chemical shielding, little work has been done to probe the shielding for a *specific* group in a large molecule. An interesting example concerns metal binding sites of nucleic acids, where the effect of the metal on ^{13}C or ^{15}N chemical shielding of bases or ribose has not been treated accurately with an empirical approach. QM/MM is ideally suited for such a problem, in which both the local structure and its fluctuations play a role.

Section II briefly describes the theory of chemical shielding calculations within the QM/MM framework, and section III applies the method to test cases that illustrate its accuracy and potential utility. The conclusions are presented in section IV.

II. Method and Implementation

We follow the standard QM/MM framework,[32b] in which the system is partitioned into two parts: the important part is treated with quantum mechanical methods, and the environment part is described with molecular mechanics methods. In the present application, the QM part is treated with either the DFT[33,42] or MP2 approach.

The chemical shielding tensor in a large molecule like a protein is usefully divided into terms that arise from the electronic structure of the atoms of interest as perturbed by the environment and additive contributions from other parts of the system. The former includes primarily the electrostatic effects arising from the partial charges on the MM atoms, and the latter includes the contribution of *anisotropic* magnetic susceptibility tensors of aromatic and carbonyl groups. For ^{13}C and ^{15}N shielding (unlike protons), which are our main concern, these latter effects are relatively small,[2d] and they are not considered in the present work except in certain cases (e.g., the water dimer); magnetic susceptibility correction could be treated, of course, by an empirical formula.[2,25] For open-shell transition metal atoms, the susceptibility is very large for high-spin systems so that their effect has to be included if they are close to the nucleus of interest.[43] Such metal atoms are considered to be

part of the QM region. Finally, there is the effect of the close contact of the atom of interest with nearby groups. In the current formulation, this effect is not included and it is the major origin of errors in the QM/MM shielding at short range. Some details of the approach are presented with the specific examples.

II.1. Electrostatic Contribution to the NMR Chemical Shielding. With the GIAO ansatz, the atomic basis functions are taken to be field dependent (London orbitals); that is,

$$\chi_\mu(\mathbf{B}) = \exp\left[-\frac{i}{2c}(\mathbf{B}\times\mathbf{R}_\mu)\cdot\mathbf{r}\right]\chi_\mu(0) \quad (1)$$

where the $\chi_\mu(0)$ is the standard Gaussian atomic orbital, **R** and **r** are the position vector of the nuclei and electrons, respectively, **B** is the external magnetic field, and c is the velocity of light.

The chemical shielding tensor, σ^N, for nucleus N is then given by the second-order response of the electronic energy E with respect to the external magnetic field **B** and nucleic magnetic moment $\mathbf{m}_N$ by the expression[11]

$$\sigma_{ji}^N = \left[\frac{\partial^2 E}{\partial B_i\,\partial m_{N_j}}\right]_{B=0} = \sum_{\mu\nu} D_{\mu\nu}\frac{\partial^2 h_{\mu\nu}}{\partial B_i\,\partial m_{N_j}} + \sum_{\mu\nu}\frac{\partial D_{\mu\nu}}{\partial B_i}\frac{\partial h_{\mu\nu}}{\partial m_{N_j}} \quad (2)$$

where σ_{ji}^N is the jith component of the shielding tensor, B_i is the ith component of the external magnetic field, and m_{Nj} is the jth component of the magnetic moment of nucleus N. On the right-hand side of eq 2, $D_{\mu\nu}$ is the atomic orbital (AO) density matrix element corresponding to the *ab initio* method employed and $h_{\mu\nu}$ is a matrix element of the one-electron Hamiltonian in the GIAO basis. The isotropic component is defined as one-third of the trace of the shielding tensor, and the anisotropy is defined as $(\epsilon_3 - (\epsilon_1 + \epsilon_2)/2)$, where ϵ_i are the eigenvalues of the symmetrized shielding tensor $(\sigma + \sigma^T)/2$; symmetrization is necessary because σ is not a symmetric tensor.

In the current implementation of QM/MM, the MM atoms polarize the wave function of the QM region as point charges and contribute to σ_{ji}^N in two ways. First, the MM atoms modify the density matrix, $D_{\mu\nu}$, and make *implicit* contribution through the first term on the r.h.s. of eq 2. Second, the MM atoms influence the derivatives of density matrix, $\partial D_{\mu\nu}/\partial B_i$, and therefore make contribution to σ_{ji}^N through the second term on the r.h.s. in eq 2; this term was *not* mentioned in previous related work,[35] although it appears to have been included in the program (TX90[44]) used in the calculations. This can be shown explicitly for the case of Hartree−Fock (HF), where the derivative of the density matrix for a closed-shell system has the form ($D_{\mu\nu}^{\mathrm{SCF}} = \sum_j^{\mathrm{occ.}} C_{\mu j}^* C_{\nu j}$):

$$\frac{\partial D_{\mu\nu}^{\mathrm{SCF}}}{\partial B_i} = \sum_p^{\mathrm{all}}\sum_j^{\mathrm{occ.}}(U_{jp}^{B_i *} C_{\mu p}^* C_{\nu j} + C_{\mu j}^* C_{\nu p} U_{jp}^{B_i}) \quad (3)$$

The $U_{jp}^{B_i}$ are the expansion coefficients of the derivative of the MO coefficients with respect to the external magnetic field; that is,

$$\frac{\partial C_{\mu p}}{\partial B_i} = \sum_q^{\mathrm{all}} U_{pq}^{B_i} C_{\mu q} \quad (4)$$

To obtain the independent occupied-virtual block of the $\mathbf{U}^{\mathbf{B}}$ matrix, the coupled-perturbed Hartree−Fock (CPHF) equations are used;[7b,11] they are (see also Ditchfield[7a])

$$(\epsilon_a - \epsilon_j)U_{aj}^{B_i} + \sum_m^{\mathrm{vir.}}\sum_l^{\mathrm{occ.}}[\langle al||jm\rangle - \langle am||jl\rangle]U_{ml}^{B_i} = I_{aj}^{B_i} \quad (5)$$

where the rhs of eq 5 is given by

$$I_{aj}^{B_i} = -\sum_{\mu\nu} C_{\mu a}^*\left(\frac{\partial h_{\mu\nu}}{\partial B_i} + \sum_m^{\mathrm{occ.}}\sum_{\sigma\lambda} C_{\sigma m}^* C_{\lambda m}\frac{\partial\langle\mu\sigma||\nu\lambda\rangle}{\partial B_i}\right)C_{\nu j} + \sum_{mn}^{\mathrm{occ.}} S_{mn}^{B_i}\langle an||jm\rangle + S_{aj}^{B_i}\epsilon_a \quad (6)$$

The redundant occupied−occupied and virtual−virtual block of the $\mathbf{U}^{\mathbf{B}}$ matrix is specified from the derivative of the orthonormal condition of the MOs,

$$U_{pq}^{B_i} + S_{pq}^{B_i} + U_{qp}^{B_i *} = 0 \quad (7)$$

In the above equations, the Latin letters indicate MO indices and the Greek letters indicate AO indices. The ϵ_i and $C_{\mu i}$ are the orbital eigenvalues and eigenvectors of the Fock matrix, respectively. The $\langle\mu\sigma||\nu\lambda\rangle$ and $\langle in||jm\rangle$ are the anti-symmetrized two-electron integrals in the AO and MO representations, respectively, and $S_{ij}^{B_k}$ is the derivative of the overlap matrix with respect to the external magnetic field.

The MM atoms make *explicit* contribution to the one-electron integral derivative with respect to the external magnetic field in eq 6,

$$\frac{\partial h_{\mu\nu}}{\partial B_k} \equiv \left\langle\frac{\partial\chi_\mu(\mathbf{B})}{\partial B_k}\middle|h\middle|\chi_\nu(\mathbf{B})\right\rangle + \left\langle\chi_\mu(\mathbf{B})\middle|\frac{\partial h}{\partial B_k}\middle|\chi_\nu(\mathbf{B})\right\rangle + \left\langle\chi_\mu(\mathbf{B})\middle|h\middle|\frac{\partial\chi_\nu(\mathbf{B})}{\partial B_k}\right\rangle \quad (8)$$

Specifically, the MM partial charges augment the one-electron operator h with an electrostatic term, $\sum_C^{N_{\mathrm{MM}}} -eQ_c/|\vec{R}_c - \vec{r}|$, where Q_c is the MM partial charge; therefore, the MM atoms contribute to the first and third term in the rhs of eq 8. It is important to emphasize that the MM contribution represented by eq 8 is for the CPHF with respect to the *external magnetic field*. Therefore, one should not confuse the present case with the earlier result[33] that the CPHF solutions with respect to the MM *nuclear displacements* contribute little to the Hessian matrix elements (although significantly to the IR intensities). In our calculations, we found that the MM contribution from eq 8 is essential for obtaining accurate values for the shielding tensors of the QM atoms. Many programs, such as Gaussian,[34] can handle point charges in energy calculations. The *implicit* MM contributions to properties such as the chemical shielding (i.e., the effect from the point charges on the converged density matrix) can be accounted for without modifying the code. However, MM atoms also make contributions through the CPHF equations; this is basically what has been added to the Gaussian program.

It is also straightforward to consider the MM contribution to the chemical shielding tensor at the DFT level if the standard current-independent exchange-correlation functional is used. In such a framework, the formulas are in the same form as that for HF, (i.e., eqs 2−7). The difference is that the CPHF eq 5 has to be replaced by the CPKS equation that includes exchange-correlation contributions.[17] The MM atoms make explicit contributions to the CPKS equations in the same fashion as in eq 8. In the SOS-DFPT approach of Malkin et al.,[6b] the MM atoms contribute indirectly by modifying the Fock matrix

elements that influence the excitation energies and the terms involving the gauge factors.[6b,15a]

For correlated wave function based method, such as MP2, the expression for the chemical shielding tensor is identical in form to eq 2. The difference is that one uses[11] the MP2 density matrix, $D_{\mu\nu}^{\mathrm{MP2}}$, often referred as the "relaxed" or "response" density matrix,[45] and its derivative with respect to the external magnetic field, $\partial D_{\mu\nu}^{\mathrm{MP2}}/\partial B_i$; i.e., eq 2 is replaced by

$$\sigma_{ji}^{N}[\mathrm{MP2}] = \sum_{\mu\nu} D_{\mu\nu}^{\mathrm{MP2}} \frac{\partial^2 h_{\mu\nu}}{\partial B_i \, \partial m_{N_j}} + \sum_{\mu\nu} \frac{\partial D_{\mu\nu}^{\mathrm{MP2}}}{\partial B_i} \frac{\partial h_{\mu\nu}}{\partial m_{N_j}} \qquad (9)$$

The MP2 density matrix is expressed in terms of the orbital eigenvalues and two-electron integrals, and the MM atoms make implicit contributions by modifying the orbital eigenvalues. The derivative MP2 density involves the derivatives of the Fock matrix elements, two-electron integrals with respect to magnetic field, and the CPHF solutions. For detailed expressions, we refer the reader to ref 11. Here, the MM atoms make contributions to the one-electronic parts of the Fock matrix derivatives and the CPHF solutions, as in eq 8. In the similar spirit, it is possible to extend the QM/MM methodology to higher correlated QM levels such as CCSD or CCSD(T).

In short, given a program that is capable of performing a QM calculation of the chemical shielding, it is rather straightforward to add the MM contributions not only at the levels of HF and DFT but also at the MP2 level. The main modification is related to the contribution from the MM atoms to the derivatives of the one-electron matrix elements in the GIAO basis with respect to the external magnetic field. This appears in the CPHF(KS) equation for HF and DFT and also in the derivative of the excitation amplitude in the case of MP2. In the current work, we implemented the QM/MM method with Gaussian98.[34]

II.2. Possible Extensions. There are several extensions that could increase the accuracy of the QM/MM shielding calculations. Only monopole interactions are included in the present implementation. More accurate treatment of the MM electrostatic effects through higher multipoles or distributed multipoles[46] can be added straightforwardly, and they all contribute only through eq 8.

Multilayer QM/MM methods have been proposed recently by a number of authors[47,48] to allow a balanced description of the polarization involving both the QM region and immediate neighbor atoms. For example, we have implemented a number of multilayer QM/MM methods where the immediate neighbor of the QM atoms is treated with either effective fragment potentials[49] (EFP) or semiempirical (SE) methods. The interaction between the QM and SE/EFP is calculated explicitly in contrast to ONIOM-like methods;[47] this is important for polar systems, such as enzymatic active sites. It would be possible to implement chemical shielding calculations in these multilayer QM/MM methods. It should be noted that, in this respect, the present methods that include polarization explicitly are to be preferred over the recipes that treat polarization effects *implicitly*.[47] Property calculations with the outer layer(s) described with force field or semiempirical method in the ONIOM-like framework is less straightforward because no general algorithm exists for computing NMR shielding tensors at those levels.

Finally, as mentioned earlier, one may combine the QM/MM method with an empirical approach[3] so that environmental influence other than electrostatics (e.g., more distant magnetic anisotropy effects[50] or the Pauli repulsion effect) are included. The influence of Pauli repulsion can also be introduced with one-electron effective potentials such as these used in the effective fragment potential method.[49]

III. Test Applications

In this section, we describe some applications that illustrate the QM/MM method for calculating shielding tensors. Since the primary goal is to compare QM/MM results with full QM calculations, only moderate basis sets of double-ζ plus polarization quality have been used in most cases. Related issues such as the effect of QM/MM partition are also considered.

III.1. Water Dimer. A number of previous studies of the water dimer used the QM/MM method to describe hydrogen bonding with one water treated by QM and the other by MM. Satisfactory results have been obtained for the geometry and energy, as well as for the vibrational frequencies.[32b,e,33] The chemical shielding of the water dimer has been studied previously by QM methods.[51] Here, comparisons are made between calculations treating the entire system by QM and by QM/MM with one water molecule described by QM and the other by MM.

The structure was first optimized with full QM, and the shielding tensors for the oxygen and hydrogen atoms were calculated as a function of the distance between the donor hydrogen and the acceptor oxygen at full QM and at QM/MM levels. All other geometrical parameters were fixed at the values in the minimum energy structure. The QM level used was B3LYP[52]/6-311G(d,p),[53] and the MM calculation used the flexible modified TIP3P model.[54] In the QM/MM calculations, either the donor or the acceptor water molecule was described with QM. The chemical shift of the two oxygen atoms and selected hydrogen atoms, relative to the isolated water molecule as the reference, was calculated. In the full QM calculations, care was taken to correct for the basis set superposition error (BSSE). The counterpoise correction[55] was carried out at each geometry by calculating the shielding of the water monomer in the presence of the basis functions on the other water molecule. The results are shown in Figure 1 as a function of the distance between the donor hydrogen and the acceptor oxygen; the value of R at the dimer minimum is 1.932 Å.

As found in a number of previous studies,[51,56] the full QM results for the dimer show that the counterpoise correction for BSSE has a significant effect on both the isotropic and anisotropic shielding of the donor and acceptor oxygen atoms. At short distances, the correction can be as large as 45 ppm for the chemical shift anisotropy (CSA) of the acceptor oxygen. The large magnitude could be due to the fact that no diffuse functions, which usually decrease BSSE, were included in the calculations. To verify this, a number of calculations with the 6-311++G(d,p) basis set were carried out. As expected, the effect of BSSE becomes much smaller; for example, it was 4 ppm compared to 45 ppm for the CSA of the acceptor oxygen at $R = 1.75$ Å when the 6-311G(d,p) basis is used. The BSSE corrected isotropic shielding of the oxygen atoms was increased by a few ppm at large R ($R > 1.95$ Å for the donor oxygen and $R > 2.5$ Å for the acceptor oxygen) and decreased at short range ($R < 1.95$ Å for the donor oxygen and $R < 2.5$ Å for the acceptor oxygen). The latter is likely to be due to the Pauli repulsion between the two water molecules, which causes a depletion of electron density between them.[2d] As depicted schematically in Figure 1, the least shielded principal components for the oxygen atoms are perpendicular to the molecular plane; the most shielded principal components, σ_{33} in Figure 1, form angles about 45° and 150°, respectively, with the two O−H

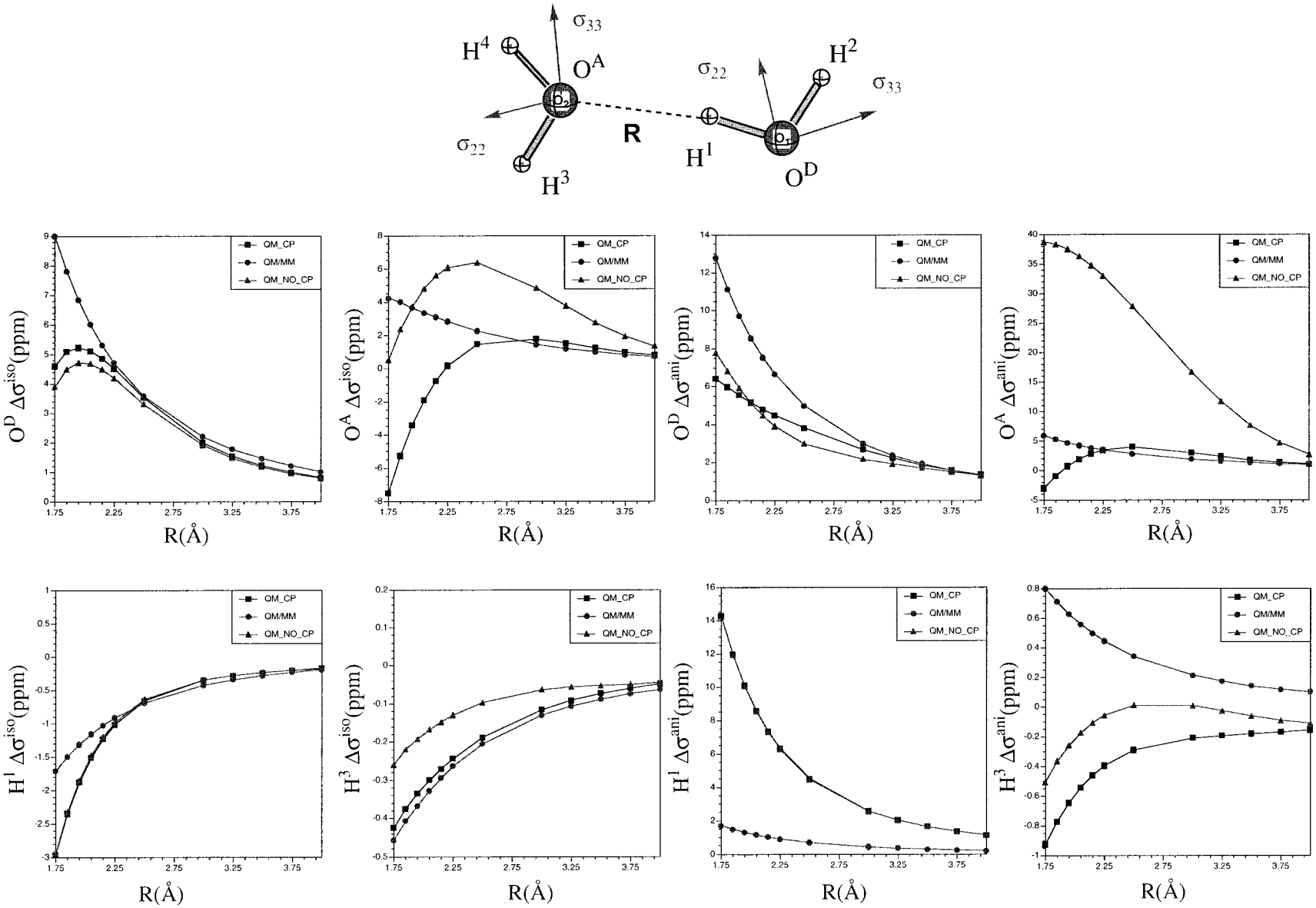

Figure 1. Comparison of the full QM and QM/MM chemical shielding parameters (in ppm) for the water dimer as a function of the hydrogen bond distance. QM is done with B3LYP/6-311G(d,p) and the MM water is described with modified TIP3P model. *R* (in Å) is the distance between the donor hydrogen (H^1) and the acceptor oxygen (O^A). The arrows indicate the directions of the shielding tensors; σ_{11} (not shown) is the least shielded component, and σ_{33} is the most shielded component. The shielding tensor components (see text for definition) are plotted with the isolated water molecule as the reference; the calculated values for the isolated molecule are 333.1/22.1 ppm for oxygen and 31.4/17.4 ppm for hydrogen. The QM_CP data are obtained with the counterpoise (CP) correction for BSSE, while QM_NO_CP results are obtained without invoking the CP correction. For H^1, the CP has very small effect on the anisotropies, so that the QM_CP and QM_NO_CP curves overlap.

bond vectors. The anisotropy of the acceptor oxygen follows a trend similar to that of the isotropic component, while that of the donor oxygen keeps increasing as the internuclear distance gets shorter. For H^1, the hydrogen bonding hydrogen, and H^3, the isotropic components decrease monotonically as the two water molecules approach each other. The anisotropy of the donor hydrogen atom increases monotonically as the internuclear distance gets shorter, while that for the acceptor hydrogen atom shows the opposite trend, but on a much smaller scale. The former was noted by Ditchfield,[51a] who pointed out that the large change in proton anisotropy is a more sensitive indicator of hydrogen bonding than the change in the isotropic shielding.

The QM/MM results are seen from Figure 1 to be satisfactory for the isotropic chemical shift at distances greater than 2.5 Å. The error becomes significant when the donor−acceptor distance is reduced further; it is as large as 7 ppm for the acceptor oxygen at the minimum distance ($R = 1.932$ Å). In general, the QM/MM results are in much better agreement with the full QM values than are the QM calculations without counterpoise correction. Also, the QM/MM results are all monotonic functions of the internuclear distance. This supports the argument that the decrease in chemical shielding at short distance is due primarily to the Pauli repulsion effect, which is not included explicitly in the evaluation of the QM/MM shielding tensor. It suggests that hydrogen bonded water molecules have to be included as part of the QM system, but that more distant ones can be treated with the QM/MM model.

For the anisotropies of the chemical shift, a similar trend is observed; i.e., the QM/MM results are close to full QM calculations at large donor−acceptor distances (down to about 2.5 Å). An exception is the anisotropy of the donor hydrogen, where a large difference (around 7 ppm at the optimum hydrogen bond distance, 1.932 Å) is observed for most distances. This can be partly explained by the magnetic susceptibility of the water molecule. The effect on chemical shift can be estimated from the McConnell equation;[29] that is,

$$\Delta\vec{\sigma} = \frac{\vec{\chi}}{r^3} - \frac{3\vec{\chi}}{r^5}\mathbf{r}\mathbf{r}^{\mathrm{T}} \tag{10}$$

where $\vec{\chi}$ is the magnetic susceptibility tensor of the perturbing group (the acceptor water molecule in our case) and $\mathbf{r}$ is the vector pointing from the center of this group to the probe nucleus. Although the $\vec{\chi}$ of water has a rather large isotropic value (about 22 ppm Å/molecule[57]), it is nearly isotropic. According to eq 10, such a magnetic susceptibility has very little influence on the isotropic shielding of the probe nucleus, but it can have a large effect on the shielding anisotropy. With the values of $\vec{\chi}$ given in ref 57, the contribution of the acceptor water on the shielding anisotropy of the donor hydrogen H^1 is calculated to be 6.8 ppm at 1.75 Å and 3.1 ppm at 2.25 Å, respectively. This is about half of the discrepancy between the full QM and the QM/MM results (12.6 and 5.4 ppm, respectively). At longer distances, the McConnell equation gives nearly the entire difference between the QM and QM/MM values; it equals 1.6 ppm at $R = 3.25$ Å and the correction given by the McConnell equation is 1.5 ppm. The residual error at smaller distance is probably due to the absence of the Pauli repulsion contribution in the QM/MM model.

III.2. *N*-Methylacetamide (NMA)−Water Complex. As another hydrogen bonded system, we examine the NMA−water complexes shown in Figures 2 and 3. This is of particular interest because NMA is the standard simple model for the protein backbone. The QM level here is B3LYP/6-311G(d,p), and the water is described with the modified TIP3P model[54] in the QM/MM calculations. For the consideration of distance dependence, the chemical shifts were calculated relative to isolated NMA and water; for the angular dependence, the chemical shifts were determined relative to the linear, coplanar NMA−water configuration.

Figures 2 and 3 show that the effect of BSSE on the ^{13}C and ^{15}N shift is much smaller than that observed for the oxygen atoms in water dimer. As was the case for the water dimer, the counterpoise correction always brings the full QM results closer to the QM/MM values. When the water molecule approaches from the side of amide proton, as in Figure 2a, only the chemical shift of the nitrogen atom is affected significantly. The least shielded principal component, σ_{11} in Figure 2, is at an angle of 20° with respect to the N−H bond vector. The directions of the principal shielding components are not much affected by the distance between the NMA and water. The principal component perpendicular to the NMA−water plane, σ_{22}, decreases as a function of the water−NMA distance, while the in-plane principal components increase as functions of the distance. The isotropic component of the N atom follows the same trend as the donor oxygen in the water dimer. The CSA of the N atom decreases as the distance decreases, while the CSA increases for the donor oxygen as the two water molecules approach each other. The QM/MM results are in good agreement with the full QM calculations, except for distances shorter than 2.3 Å where the Pauli repulsion effect becomes important.

The dependence of the chemical shift on the N−H···O angles of the hydrogen bond between the NMA and water are shown in Figure 2b. In the first case, the NMA−water hydrogen bond deviates from linearity as the water molecule moves in the NMA plane. In the second case, the water moves out of the NMA plane with a lone pair pointing to the amide proton. Sitkoff et al.[31] discussed the angular dependence of the shielding of the amide proton in similar systems using the SOS-DFPT/IGLO-III approach. They found that the DFT result could be fitted well by the Buckingham formula[27] only if a water model with lone pairs (e.g., ST2[58]), rather than a simple three-site model (e.g., TIP3P), was used to treat the electrostatic polarization. To determine if the same behavior is found with the QM/MM approach, we tested both the ST2 and TIP3P model to describe the MM water. The computed chemical shifts for both the nitrogen and the amide proton are shown in Figure 2b. For both the in-plane and the out-of-plane cases, the QM/ST2 and QM/TIP3P calculations give very similar results. Both calculations give satisfactory isotropic proton chemical shifts as functions of the bending angle. The CSA of the amide proton in the out-of-plane case is poorly described by both QM/MM calculations. The change in the QM/MM results as a function of the bending angle is too small, as compared with the full QM values. This presumably is due to the fact that the oxygen−nitrogen distance becomes rather short as the bending angle increases; it is about 2.8 Å when the bending angle is 60°, and Pauli repulsion is likely to be important. The chemical shifts of the nitrogen atom are only qualitatively reproduced by the QM/MM calculations. For the in-plane case in the full QM calculations, the perpendicular principal component, σ_{22}, decreases significantly, and the CSA increases significantly, as a function of the angle θ. In the QM/MM calculations, the calculated changes in the perpendicular principal component are smaller than the corresponding QM values, which results in too small an angular dependence for the CSA. For the out-of-plane case, the largest change occurs in the most shielded component, σ_{33}. The calculated changes in both the isotropic and anisotropic com-

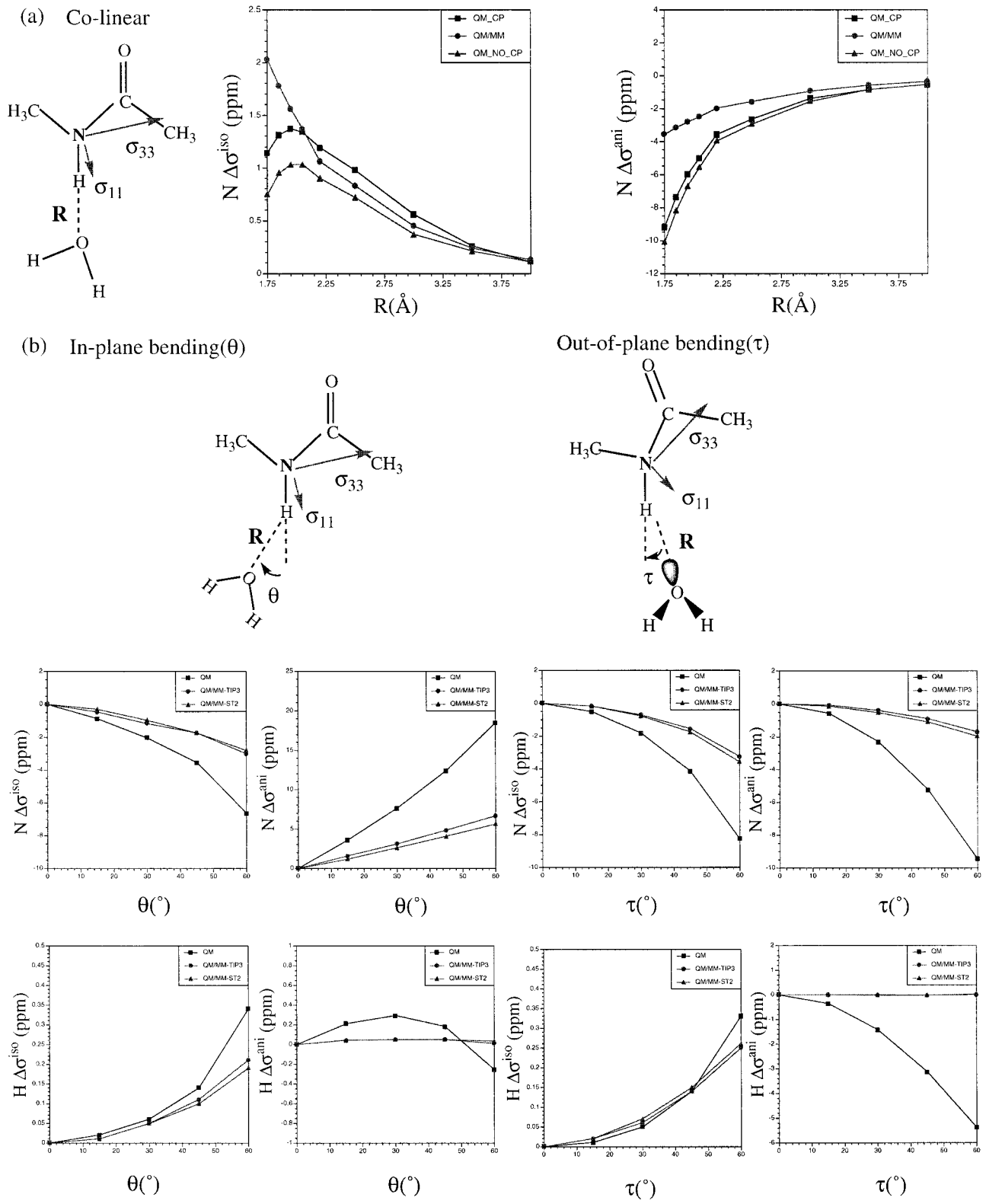

Figure 2. Comparison of the full QM and QM/MM chemical shielding parameters (in ppm) for the *N*-methylacetamide (NMA)−water complexes as the water approaches the amide proton. QM is done with B3LYP/6-311G(d,p), and the MM water is described with the modified TIP3P model. The arrows indicate the directions of the shielding tensors; σ_{11} is the least shielded component, and σ_{33} is the most shielded component. In (a), the N−H···O(water) is kept linear as the HN···O distance (R) varies. The shielding components (see text for definition) are measured relative to the separate NMA and water; the shielding is 139.4/125.6 ppm for the nitrogen atom. The QM_CP set of results are obtained with the counterpoise(CP) correction, while QM_NO_CP are obtained without invoking the CP correction. In (b), R is fixed at 2.20 Å, as the N−H···O angle varies with either the water moving in the NMA plane (characterized by the angle θ) or out of the NMA plane (characterized by the angle τ). The chemical shielding parameters are measured relative to the result for linear H−N···O.

ponents from QM/MM calculations are significantly smaller than the corresponding QM values.

As the probe water molecule approaches the carbonyl group (see Figure 3), the chemical shift of both the carbonyl group

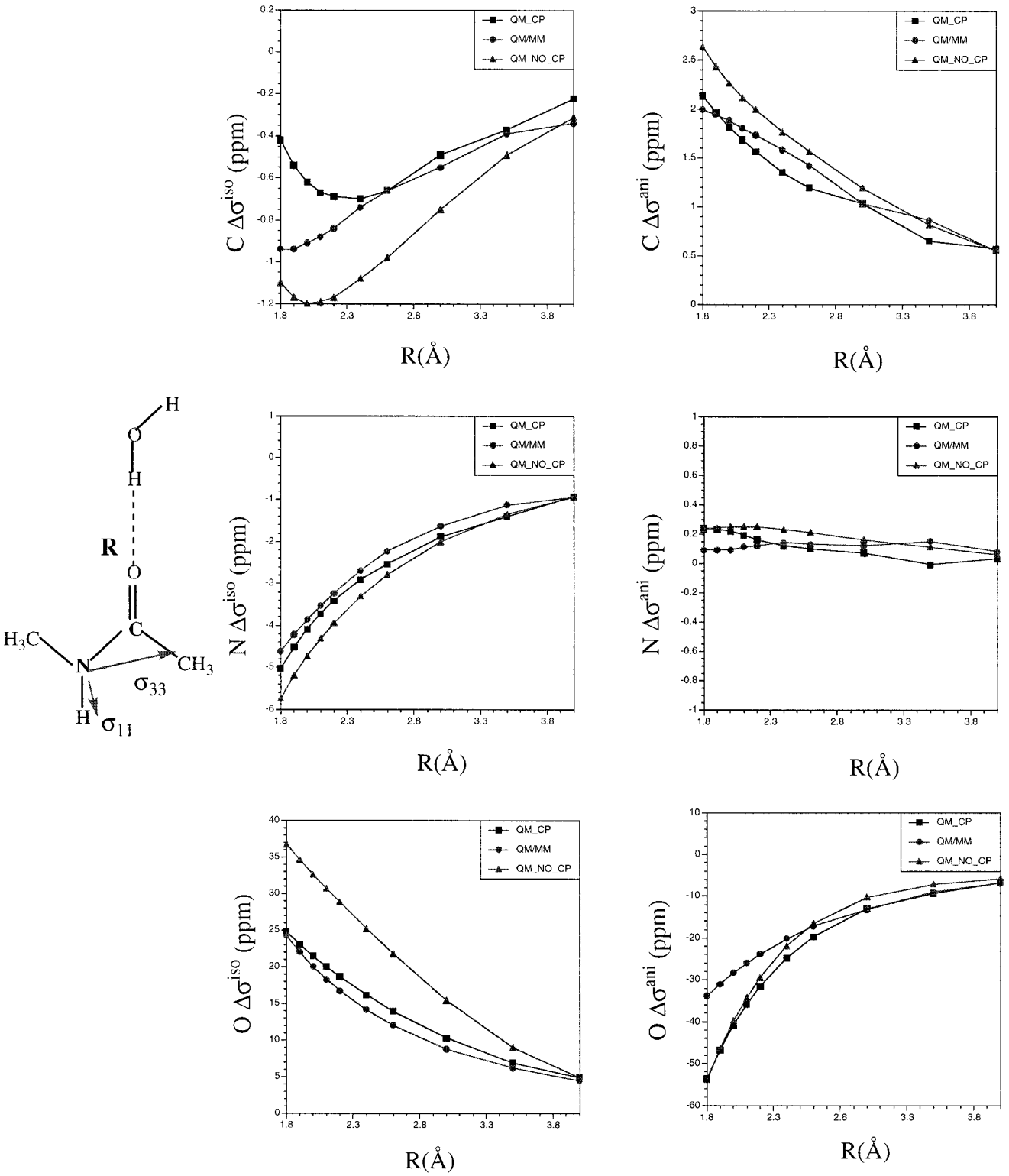

Figure 3. Comparison of the full QM and QM/MM chemical shielding parameters (in ppm) for the *N*-methylacetamide (NMA)−water complexes as the water approaches the carbonyl group. The O(water)−H···O(NMA) angle is linear in the calculations. The notations correspond to that in Figure 2a. The absolute shielding for the carbonyl C, O, and N in isolated NMA are equal to 14.9/113.8, −76.3/661.8, and 139.4/125.6 ppm, respectively.

and the nitrogen atom are affected substantially. For the carbon atom, the isotropic component decreases as the water approaches the carbonyl group, and starts to increase at distances shorter than 2.3 Å. The chemical shifts of the oxygen and nitrogen atoms, on the other hand, are monotonic functions of the distance. The signs of the chemical shift for both the carbon and nitrogen atoms are negative, in contrast to the case where the water approaches from the NH side (Figure 2). This is consistent with the different directions of electronic polarization in the two cases. The trend of the chemical shifts of the carbonyl oxygen atom is similar to that of the acceptor oxygen in the water dimer (Figure 1). The change in the CSA for the oxygen atom is on the order of 60 ppm, while those for the nitrogen and carbon atom are much smaller in magnitude. The QM/MM results are in good agreement with the full QM calculations, as seen in Figure 3, except for short distances.

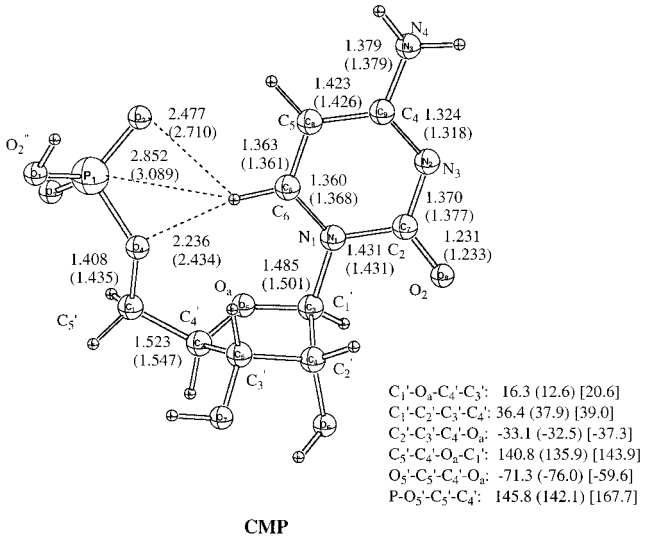

CMP

Figure 4. The structure of cytosine monophosphate (CMP) optimized with the B3LYP/6-31G(d) method and the QM/MM method (numbers in parentheses). In the QM/MM geometry optimization, partition Scheme 1 is used; i.e., only the base is included as the QM part (see text). The number in brackets are averaged values found in the NMR structure of the P5B stem-loop of the *Tetrahymena* group I intron and leadzyme.

In summary, we have found that QM/MM yields good chemical shielding results for hydrogen bonded systems at distances larger than 2.5 Å. The deviation from full QM calculations at shorter distances is due to the neglect of Pauli repulsion and the magnetic susceptibility of the nearby group in the current QM/MM model. One advantage of using QM/MM to describe environmental effect is that BSSE can be avoided. This is significant, especially for oxygen atom when a medium size basis set is used.

III.3. Nucleic Acid Bases. *III.3.1. Cytosine Monophosphate (CMP).* The chemical shielding tensors of atoms in nucleic acid bases can give important structural information, such as the protonation state of the base, the base pairing/stacking pattern, hydrogen bonding with water or protein, and binding modes of metal ions. As the first example, we investigate the effects on the base atoms from the backbone atoms, i.e., the ribose and the phosphate, all in vacuum. Specifically, we use the QM/MM method to calculate the shielding tensors for the base atoms in cytosine monophosphate (CMP). In both the full QM and the QM/MM calculations, the QM method employed is B3LYP with the 6-31G(d) basis set.[59] Two different QM/MM partitions were tested. In the first partition scheme, only the base atoms are included in the QM region and a link atom is introduced between the base N_1 atom and C_1' of the ribose. In the larger partition scheme, the QM region is extended to include C_1' and the anomeric oxygen atom O_a of the ribose. The MM part is treated with the CHARMM22 force field for nucleic acids.[60] The QM optimized structure and the important geometrical parameters are shown in Figure 4, and the calculated shielding tensors are summarized in Table 1. The geometry is similar to that typically found in nucleic acids. As examples, we consider the geometries of nine cytosines in two experimental nucleic acid structures, the P5b stem-loop of the *Tetrahymena* group I intron and a lead-dependent ribozyme. The structure of the former was determined by NMR,[61] while that of the latter was from X-ray crystallography at 2.7 Å resolution.[62] The distance between the C_6-hydrogen in the base and the O_5' in the ribose varies between 2.10 and 2.54 Å with an average of 2.37 Å. The distance between the same hydrogen and the phosphorus ranges from 3.11 to 3.69 Å (with an average of 3.38 Å). These values can be compared to the corresponding values in Figure 4, which are 2.24 and 2.85 Å at the QM level, respectively. Also shown in Figure 4 are several dihedral angles that characterize the conformation of the ribose and the orientation of the phosphate group. The conformation of the ribose from the QM calculation is similar to those found in the P5B stem-loop and the leadzyme, with differences in dihedral angles of a few degrees. The orientation of the phosphate group has a larger variance in these two nucleic acids. The $O_5'-C_5'-C_4'-O_a$ dihedral angle ranges from $-19.6°$ to $-93.7°$ with an average of $-59.6°$. The $P-O_5'-C_5'-C_4'$ dihedral angle ranges from 152.9° to 179.5° with an average of 167.7°. The corresponding value in the B3LYP optimized CMP is $-71.3°$ and 145.8°, respectively.

Despite the small basis set, the QM results are within the experimental range. For instance, the isotropic shifts of N_1, N_3, and N_4 are 167.4, 215.0, and 73.8 ppm, respectively, relative to the value of 255.0 ppm for ammonia (also calculated with B3LYP/6-31G(d)). These values can be compared to the shielding in cytidine nucleoside measured in DMSO; the corresponding values are 151.8, 207.9, and 93 ppm, respectively.[63] QM/MM calculations were performed for the shielding tensors at the QM optimized structure. The QM/MM computed shielding tensors, both the isotropic components and the anisotropies, are in good agreement with the full QM results, particularly when the large partition is used. With the small partition scheme, the shielding for N_1 is in poor agreement, which is not unexpected since N_1 is at the QM/MM boundary. This problem is alleviated in the large partition in which the QM/MM boundary is away from N_1, and the shielding for N_1 is in excellent agreement with the full B3LYP result. By using the large QM region, the CSA of O_2 is also greatly improved; i.e., from 423.8 ppm with the small partition to 464.7 ppm with the large QM partition, very close to the full QM result (462.4 ppm). Excluding N_1 in the small partition scheme, the largest absolute error between QM/MM and full QM shielding is 2.5 and 1.7 ppm for the small and the large QM/MM partition, respectively, and the RMS errors are 0.8 ppm for both partitions. To demonstrate the importance of the MM environment, the calculated shielding excluding the MM atoms are also given in Table 1. The MM atoms contribute substantially to the shielding of the base atoms; typical values are 5−10 ppm, but they can be as large as 27 ppm for O_2.

The above test and observation demonstrate that the effect of the environment on chemical shielding can be described accurately with a point charge MM model in this case. Part of the reason is that a very good structure, obtained at the full B3LYP/6-31G(d) level, is used in the QM/MM single-point calculation. In actual applications, one would usually employ the QM/MM optimized geometry, which is different from the full QM structure. We have also performed QM/MM optimization for CMP with the small partition scheme. This was carried out with the CADPAC/CHARMM program[42] at the B3LYP/6-31G(d)/CHARMM level. Some important geometrical parameters are shown in Figure 4 for comparison with the full QM results. In general, the structure at the QM/MM level is rather similar to the full QM prediction, except that the phosphate group moves a bit farther from the base. As shown in Table 1, the QM/MM shieldings calculated at the QM/MM optimized structure are also in general agreement with the full QM results, although not as close as the ones calculated with the QM optimized structure. The largest absolute error increased

TABLE 1: Computed Absolute Chemical Shielding Parameters (in ppm) for Heavy Atoms of the Base in Cytosine Monophosphate (CMP)[a]

atom[b]	full QM	QM/MM**1**	QM/MM**1** opt	QM/MM**2**	no MM
N_1	87.6/131.7	100.2/107.3	108.2/119.2	87.3/140.4	111.6/99.2
C_2	43.4/67.9	43.1/71.3	42.7/73.6	43.8/69.3	45.7/74.8
O_2	11.8/462.4	12.2/423.8	17.4/426.9	10.9/464.7	−15.6/457.1
N_3	40.2/262.1	40.9/263.4	41.6/257.9	39.3/262.3	30.7/278.0
C_4	33.7/147.7	33.6/148.5	34.3/147.6	34.3/147.7	33.2/148.0
N_4	181.2/86.5	181.6/85.5	183.0/86.8	182.2/86.0	175.2/84.0
C_5	102.5/105.6	103.8/105.6	101.1/111.4	103.4/105.0	104.2/101.7
C_6	45.7/170.4	43.2/165.0	41.3/167.7	47.4/172.1	51.8/146.0
max error[c]		2.5	5.6	1.7	27.4
RMS error[c]		0.8	2.3	0.8	7.6

[a] In both full QM and QM/MM calculations, the QM is B3LYP/6-31G(d). The MM corresponds to the CHARMM22 force field for nucleic acids. Bold faced numbers (e.g., QM/MM**1**) indicate the QM/MM partition scheme (see text). In the calculations, the full QM optimized geometry has been used except for "QM/MM**1** opt" where the QM/MM optimized geometry was used. For the shielding results, the number before the slash is the isotropic component, and the number after the slash is the anisotropy (see text). [b] For the atomic numbering scheme, see Figure 4. [c] For the isotropic component only. For QM/MM results with partition 1, the data for N_1 is excluded since N_1 is expected to be poorly described if the small QM/MM partition is used.

from 2.5 to 5.6 ppm, and the RMS error increased from 0.8 to 2.3 ppm, again excluding N_1.

III.3.2. Base Pairing and Stacking. The effects of base pairing and base stacking on the chemical shift are also of interest. We have calculated two examples to examine the accuracy of the QM/MM approach. One is the UG base pair and the other is the UC base stack. The geometries are taken from the averaged NMR structure of the P5b stem-loop of the *Tetrahymena* group I intron from the Protein Data Bank (PDB). The structure is shown in Figure 5; no energy minimization was performed. The QM level used was B3LYP/6-311+G(2d,p), and MM was the CHARMM22 force field for nucleic acid.[60] The base, whose shielding is listed, is described by QM in the QM/MM calculation. The results are given in Table 2. They compare full QM and QM/MM with the values for the isolated bases.

For the UG base pair, the largest chemical shifts, relative to the isolated base with the same geometry, are on the order of 10 ppm. They occur for the nitrogen and oxygen atoms that are close to the pair partner, i.e., N_3 in U13, O_2, O_4 in U12 and O_6 in G6 (see Figure 5). The changes in the ^{13}C shielding are smaller in magnitude (on the order of 2 to 3 ppm). The QM/MM shielding is in good agreement with the full QM results for most atoms, except for N_3 in U13 and O_6 in G6, which are involved in a very short hydrogen bond (1.832 Å). This is not unexpected from the water dimer results. The QM/MM results for these two atoms have the correct trend compared to the isolated bases, but the errors are larger than those for the other atoms; the errors are around 5 ppm in the isotropic shielding components and 20 ppm for the shielding anisotropies. For example, the isotropic shielding for O_6 in G6 is −13.5 and −9.5 ppm at the QM and QM/MM level, respectively, as compared with the value of −47.2 ppm in the isolated base. The corresponding anisotropy is 492.2, 508.3, and 558.7 ppm, respectively, for the three cases. For the other hydrogen bond, which is longer (2.223 Å), the QM/MM isotropic components are in better agreement with the full QM calculations, but there are still notable errors in the anisotropies. For instance, the isotropic shielding for O_2 in U13 is 13.3, 10.2 ppm at the QM and QM/MM level, respectively, as compared with the value of −27.9 ppm in the isolated base. The corresponding anisotropy is 382.8, 388.4, and 434.9 ppm, respectively, for the three cases. The atoms involved in hydrogen bonds have by far the largest changes due to base pair formation.

For the UC base stacking, the nitrogen and oxygen atoms have changes on the order of a few ppm, while those for carbon are less than 1 ppm. The effects on the proton shielding (not shown) are very small in this particular case, presumably due to the rather long distance between the two bases (∼3.5 Å). The QM/MM shielding is generally between the full QM value and that of the isolated base. For example, the isotropic shielding for N_1 in U13 is 92.3 and 92.5 ppm with full QM and QM/MM calculation, respectively; that in the isolated base is 98.2 ppm. The corresponding CSA values are 92.4, 90.4, and 79.2 ppm, respectively. In some cases, the difference between QM and QM/MM results is significant. For instance, the isotropic shielding for N_4 in C12 is 156.7 and 162.2 ppm at the QM and QM/MM level, respectively. For N_3 in C12, the isotropic shielding at the QM/MM level, −11.1 ppm, is rather close to the QM value of −11.9 ppm. The anisotropy, by contrast, is only qualitatively reproduced; the value is 300.6 and 295.8 ppm, at the QM and QM/MM level, respectively. Significant portion of the base stacking effect on shielding is electrostatic in nature, which is treated well by the QM/MM method. The ring current effect should be responsible for most of the remaining discrepancies; they are not included in the present QM/MM model.

To summarize, we have found that with proper partitioning, the QM/MM calculations give satisfactory corrections for the environmental effects arising from the phosphate and ribose backbone, and from hydrogen bonding. For base stacking, the example given here indicates that between 50% and 68% of the stacking effect on chemical shielding of the base atoms is electrostatic in origin. Whether this holds more generally for base stacking will be investigated separately in a more detailed study. Other factors, particularly the ring current effects, have to be taken into account if highly accurate shielding results are desired.

III.4. Metal Ion Effects. Metal ions play essential structural and functional roles in proteins[64] and nucleic acids.[65] In proteins, several types of metal ion motifs have been recognized: catalytic, structural, and cocatalytic.[64,66] Well-known examples include zinc-fingers,[67] horse liver alcohol dehydrogenase,[68] metallothionein,[69] and aspartate transcarbamoylase.[70] In nucleic acids, they are involved in the folding of RNA and in maintaining the structure;[71] in ribozymes, metal ions appear to be directly involved in the catalytic functions.[72] However, it is not always straightforward to determine the positions of the metal ions in RNA by X-ray diffraction. Na^+ and Mg^{2+} are usually distinguished from water only by the nature of the ligands. Also, metal ions have a number of possible binding modes and the one present in the crystal may not be the one in solution. For systems that have been analyzed by NMR, computed chemical shielding can aid in determining the binding

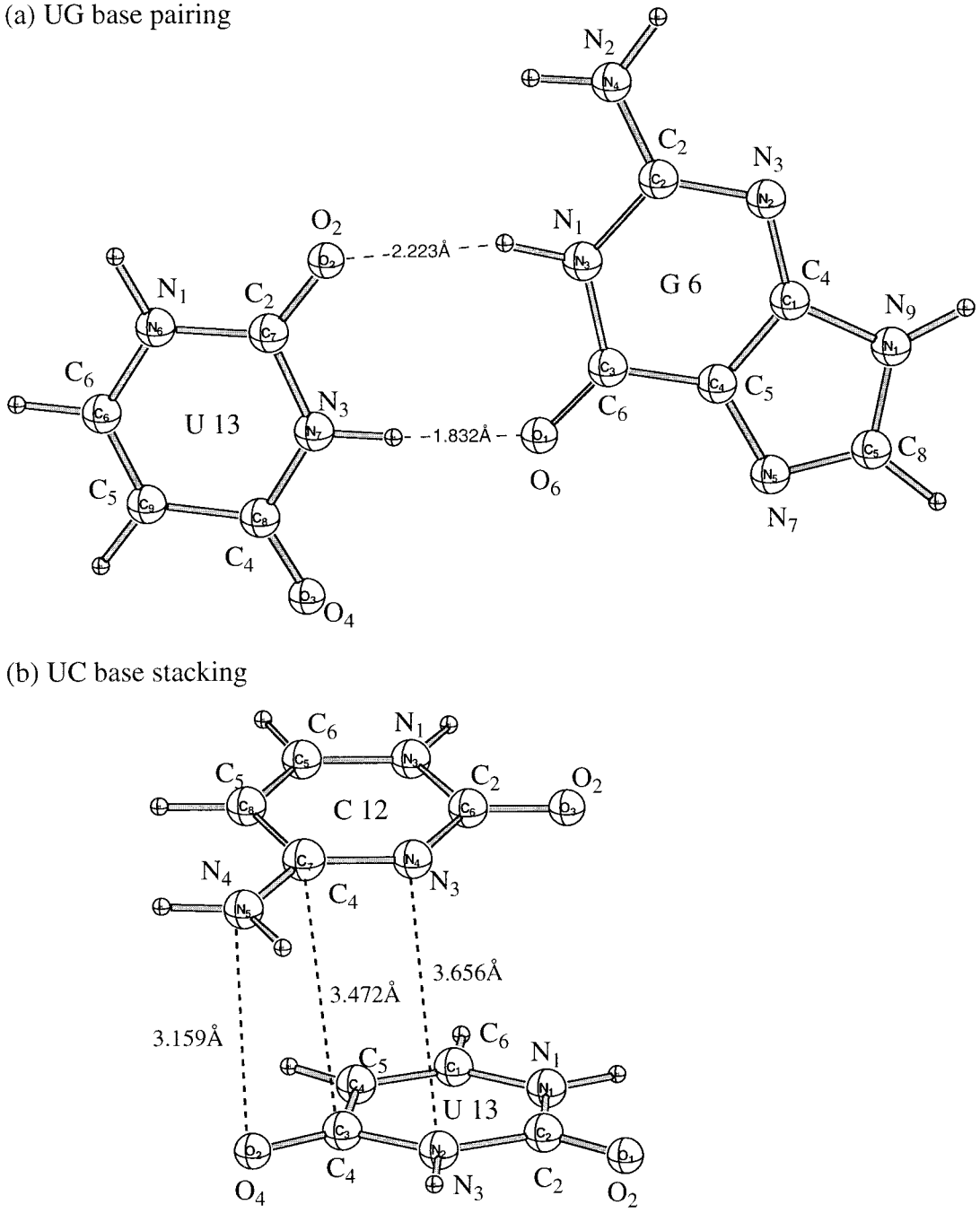

Figure 5. Geometry used for the full QM and QM/MM chemical shielding parameter calculations for UG base pairing and UC base stacking.

mode, position, and identity of the metal ion, to supplement the X-ray data or to provide binding information without X-ray data.

III.4.1. Imidazole−Metal Ion Interaction. We consider imidazole interacting with a solvated metal ion and compare it with imidazole plus a small water cluster $(H_2O)_n$ ($n = 1, 3$). The metal ions selected are Mg^{2+}, Ca^{2+}, and Pb^{2+}. The lead ion was chosen since it plays an essential role in a small ribozyme,[73] which is currently under theoretical study. In both the QM/MM and the full QM calculations, the QM method is B3LYP. The basis set for the main group elements is 6-31G(d); effective core potentials (ECP) and associated basis sets from Dolg et al.[74] have been used for Ca^{2+}, and these from Hay et al.[75] are used for Pb^{2+}. In the QM/MM calculations, the waters are treated with the modified TIP3P model. Several calculations with the metal ions described as point charges are also carried out for comparison. The examples are designed to investigate the following questions. First, can one represent the "uninteresting" ligands of the metal ion (solvent water molecules in this case), or even the ion itself, by MM when calculating the shielding of atoms in molecules interacting with the metal ion? Second, can one distinguish different metal ions and water binding to imidazole by examining the chemical shift of the later, and how significant are the differences?

The optimized structures used in the calculations are shown in Figure 6. For the complexes with Mg^{2+} or Ca^{2+}, the metal ions adopt hexacoordination as expected. For Pb^{2+}, however, we were not able to find symmetric hexacoordinated species. Putting four or five water molecules around the lead ion yields structures with one or two dissociated water molecules. Therefore, it appears that lead ion prefers to be four or even three coordinated. We have found similar trend in pure lead ion−

TABLE 2: Computed Absolute Chemical Shielding Parameters (in ppm) for Heavy Atoms in the UG Base Pair and UC Base Stack[a]

	UG pair			UC stack		
atom[b]	full QM	QM/MM	isolate base	full QM	QM/MM	isolate base
U−N_1	100.3/74.8	100.2/76.5	98.2/79.2	92.3/92.4	92.5/90.4	98.2/79.2
U−C_2	17.5/79.9	18.2/81.1	20.7/75.8	20.8/77.7	20.8/75.6	20.7/75.8
U−O_2	13.3/382.8	10.2/388.4	−27.9/434.9	−30.0/438.0	−31.4/440.1	−27.9/434.9
U−N_3	59.3/100.8	64.5/77.9	67.4/57.2	66.6/60.3	67.1/60.1	67.4/57.2
U−C_4	12.3/108.2	13.0/107.8	12.2/109.5	10.6/116.0	10.6/112.6	12.2/109.5
U−O_4	−127.5/643.7	−131.3/642.6	−111.5/605.9	−92.5/580.4	−83.0/563.6	−111.5/605.9
U−C_5	70.9/113.3	71.5/113.8	73.7/111.0	74.9/111.3	76.9/103.7	73.7/111.0
U−C_6	38.7/146.1	38.2/147.5	36.2/151.1	35.4/155.9	33.2/156.3	36.2/151.1
N_1/N_1	83.4/90.3	83.9/74.7	84.7/67.5	90.6/97.4	90.7/97.1	89.1/100.2
C_2/C_2	21.2/116.4	21.4/116.7	22.1/115.6	18.1/83.3	18.6/79.3	18.2/80.1
N_2/O_2	182.9/101.3	182.6/102.7	183.5/104.5	−46.6/439.6	−55.3/450.4	−60.6/457.6
N_3/N_3	46.3/284.6	46.5/285.2	47.4/284.0	−11.9/300.6	−11.1/295.8	−14.7/301.4
C_4/C_4	22.3/118.7	22.6/118.2	23.7/116.6	7.5/172.7	7.7/169.4	7.7/169.6
N_9/N_4	84.6/86.0	84.5/86.5	84.5/86.9	156.7/94.7	162.2/98.7	167.0/100.3
C_5/C_5	58.9/116.4	58.8/116.3	58.1/116.4	85.2/109.6	86.7/106.1	86.8/105.5
C_6/C_6	20.9/95.7	21.1/97.0	22.0/92.9	37.0/152.8	36.5/153.0	36.1/153.9
G−O_6	−13.5/492.2	−9.5/508.3	−47.2/558.7			
G−N_7	−28.3/409.1	−28.5/409.4	−28.8/409.0			
G−C_8	45.9/98.6	45.9/98.8	46.1/98.4			

[a] QM in both full QM and QM/MM is B3LYP, and MM is the CHARMM 22 force field for nucleic acids. Basis set is 6-311+G(2d,p). The geometries are taken from the averaged NMR structure of P5b stem-loop of the *Tetrahymena* group I intron (see Figure 5). Only results for N, C, and O are shown. For the format of the shielding results, see Table 1. [b] The symbol before the dash gives the base name. In cases where there are two atoms symbols, the one before the slash is for G in the UG base pair, and the one after the slash is for C in the UC stack.

water complexes (results not included). It is interesting to see that the lead ion prefers to have an empty side in its coordinate sphere. This can be explained by the electronic configuration of the lead ion, which is nominally s^2. It is expected that s^1p^1 configuration mixes significantly such that the lone pair lobe is strongly polarized and *not* spherically symmetric. As a result, the lead ion prefers to bind to other electron donor from either the opposite side of the lone pair or in the plane perpendicular to the lone pair to minimize the repulsion. This is exactly what was found (see Figure 6). Examination of the Cambridge Structural Database[76] shows a number of structures with similar coordination sphere to that found here; examples are $Pb(NH_2 \cdot Ph \cdot COO^-)_2$, $PbBr_2(OSMe_2)_2$, and $Pb(SCN)_2(OSMe_2)_2$.

The differences in shielding parameters for imidazole binding with different metal ions and water cluster are shown in Table 3; the imidazole by itself is also shown for comparison. In evaluating the differences, we describe only the full QM results. There are significant differences in the imidazole shielding among these systems; the largest differences occur for N_4 to which the ligands are coordinated. For the three metal ion complexes, the different metal ion radii result in different metal−N_4 distances, 2.149, 2.301, and 2.445 Å, for Mg^{2+}, Pb^{2+}, and Ca^{2+}, respectively. This is reflected in the trend of the isotropic N_4 shielding, 46.0, 36.6, and 29.7 ppm, for the three metal ion complexes, respectively. The CSA of N_4 in the Pb^{2+} complex (236.7 ppm) is smaller than that for Mg^{2+} (280.2 ppm) and Ca^{2+} (297.4 ppm). This is partly due to the asymmetric coordination sphere of the lead ion, in contrast to that of the other two metal ions. The differences in the shielding of the other imidazole heavy atoms are much smaller; they are on the order of a few parts per million. Comparing the metal ion−imidazole species to the water−imidazole complexes, the largest difference occurs, as expected, on the N_4 atom that is directly coordinated to either the metal ion or a water molecule. Nevertheless, large differences in the shielding, on the order of 10 ppm, are found for all the heavy atoms that are not directly involved in the coordination. The two water−imidazole complexes also exhibit rather different shielding for C_3, N_4, and C_5, reflecting the different extent of electronic polarization in the two species, which is indicated by the Mulliken charges on N_4 in Figure 6.

The largest discrepancies between QM/MM and full QM calculations occur on the N_4 atom in imidazole, which is directly coordinated to the metal ions. This is partly due to the limitation that no charge transfer (CT) is allowed between metal ion and water, as indicated by the Mulliken charges shown in Figure 6. Evidently, the metal ion is more positive when the surrounding water molecules are treated with MM. This results in a stronger electronic polarization at the coordinated atom, N_4, in the imidazole, as indicated by its Mulliken charge in Figure 6, which in turn influences the value of the chemical shielding. If we simply use point charges of +2.00 to describe the metal ions, indicated as the "QM/MM-2" calculations in Table 3, the Mulliken charges on N_4 become even more negative and the shielding deviates much more from the full QM result. Comparing the three ion−imidazole complexes, we see that the error from the QM/MM calculation decreases as the metal−N_4 distance increases. Since the differences in the full QM and QM/MM Mulliken populations on N_4 are very similar in the three species, this suggests that part of the error in the QM/MM calculation comes from the Pauli repulsion between the ligand waters and the imidazole, which has sensitive distance dependence. It is also interesting to note that although the QM/MM calculations give larger isotropic shielding than full QM in most cases, it gives a smaller isotropic shielding in the case of Pb^{2+}·imidazole complex. For atoms that are far from the metal ions, the QM/MM calculations give good results compared to the full QM values, even if the metal ion is described as a point charge of +2.00. A point charge of +1.00 is close to the Mulliken charge from the QM calculation, and use of that charge for the metal ion in the QM/MM calculation yields a Mulliken charge on N_4 that is much closer to the QM value (Figure 6). The shielding (not shown), however, is much closer to that in the isolated imidazole. It was found that a value of +1.60 for the metal ion gave good shielding for N_4. The chemical shielding parameters for the other heavy atoms are in worse agreement with the QM values, as compared with the QM/MM calculations

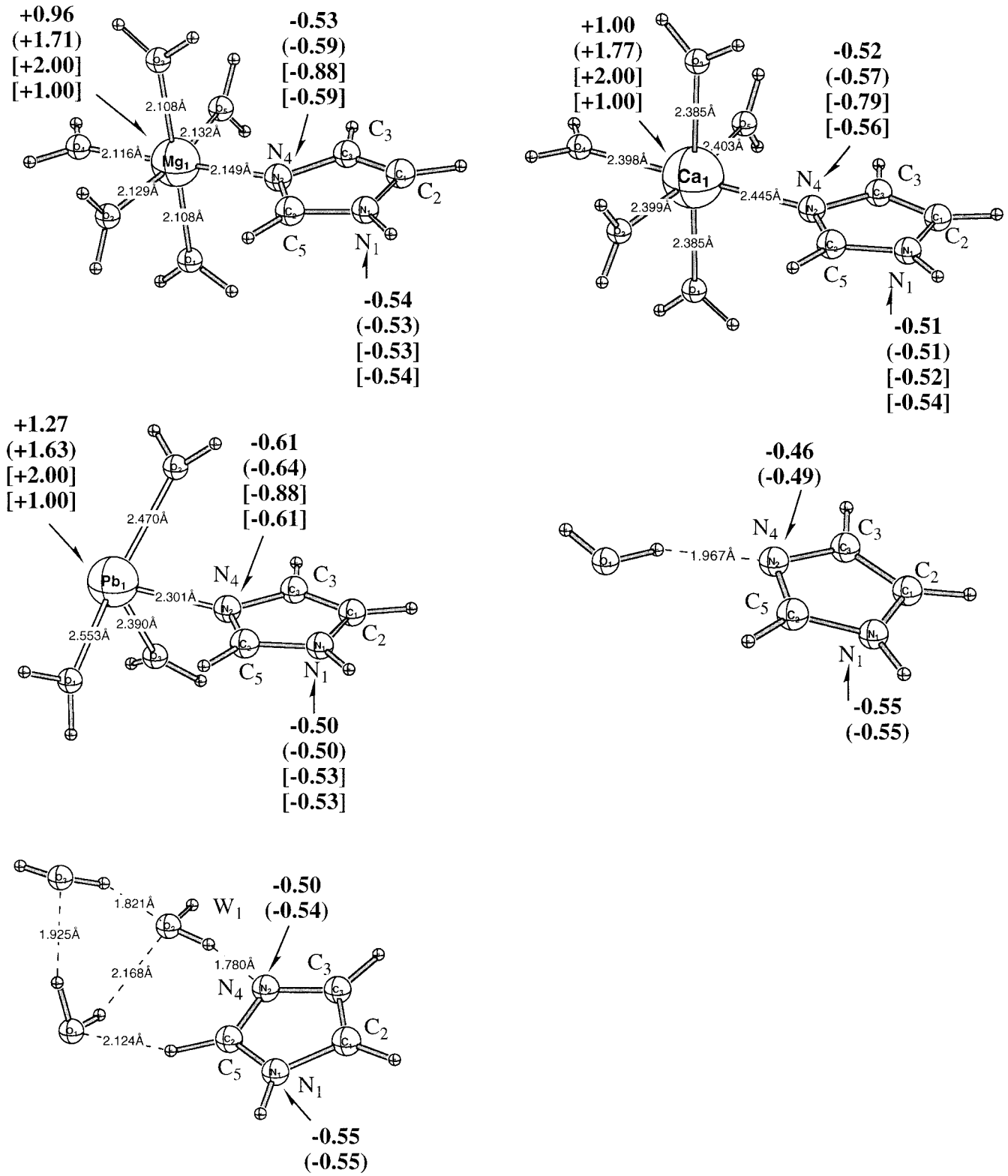

Figure 6. Structures of imidazole interacting with solvated metal ions and a small water cluster, all optimized by full QM at the B3LYP level. For all main group atoms except Ca^{2+}, the 6-31G(d) basis set is used. For Pb^{2+}, the Hay−Wadt ECP and the associated basis set (ref 75) is used. For Ca^{2+}, the Dolg ECP and associated basis set (ref 74) is used. The numbers in bold face are Mulliken charges. The numbers without parentheses or brackets are obtained at the full B3LYP level; the numbers in parentheses are from QM/MM calculations with MM water molecules; and the numbers in brackets are from QM/MM calculations with both the metal ions and water molecules treated with MM.

using a point charge of +2.00 for the metal ion. This suggests that the metal ion must be treated quantum mechanically in chemical shift calculations for its ligands.

For the water−imidazole complex, the MM description of the water molecules yields satisfactory results for the isotropic shielding. From the water dimer and NMA−water complexes, we expect that Pauli repulsion makes significant contributions at short hydrogen bond distances. For the N_4 atom in the imidazole, which forms a rather strong hydrogen bond with water, the isotropic component from the QM/MM calculation is rather similar to the full QM value, but the CSA from the two calculations deviate substantially.

TABLE 3: Computed Absolute Chemical Shielding Parameters (in ppm) for Atoms of Imidazole Binding to Solvated Metal Ions or a Water Cluster[a]

	Mg^{2+}				Ca^{2+}		
atom[b]	full QM	QM/MM	QM/MM-2	imidazole	full QM	QM/MM	QM/MM-2
N_1	90.6/151.2	88.3/159.4	90.5/154.9	106.5/117.0	92.4/148.1	90.9/152.4	91.9/150.0
C_2	73.5/118.4	72.7/122.7	73.0/120.6	83.0/106.0	74.7/118.9	73.9/121.0	73.7/119.2
C_3	69.0/110.3	69.2/110.0	71.7/109.1	65.6/90.6	70.0/109.6	71.3/110.1	70.9/109.2
N_4	46.0/280.2	65.5/249.0	68.1/252.2	−7.6/397.3	29.7/297.4	34.3/282.5	55.6/281.5
C_5	62.0/105.3	61.5/107.8	64.7/105.5	67.2/109.1	63.0/104.1	63.2/105.6	64.6/103.6

	Pb^{2+}			H_{2O}		$(H_2O)_3$	
	full QM	QM/MM	QM/MM-2	full QM	QM/MM	full QM	QM/MM
N_1	88.7/159.5	88.6/162.9	91.3/153.0	106.0/120.6	106.3/119.2	104.9/123.0	105.8/120.7
C_2	71.4/121.7	73.0/122.6	72.8/119.6	82.5/104.8	83.0/105.1	82.8/104.2	83.1/104.5
C_3	74.1/109.6	74.8/112.3	71.8/110.5	63.3/98.3	63.5/97.7	70.0/108.5	69.1/109.5
N_4	36.6/236.7	17.2/226.4	64.2/256.8	1.8/362.8	3.9/375.9	13.7/336.0	10.0/361.7
C_5	62.3/113.6	63.9/115.2	63.9/108.3	68.5/109.4	68.5/109.2	58.4/112.2	61.8/104.4

[a] QM in both full QM and QM/MM is B3LYP. For all main group atoms except Ca, the 6-31G(d) basis set is used. For Pb, the Hay−Wadt ECP and the associated basis set (ref 75) is used. For Ca, the Dolg ECP and associated basis set (ref 74) is used. In the QM/MM calculations, the water molecules around the metal ions are treated with the modified TIP3P model. In the QM/MM-2 calculations, the metal ions are treated with point charges of +2.00. For the format of the shielding data, see footnote of Table 1. [b] For atomic numbering scheme, see Figure 6.

III.4.2. 1′-Deoxyribose−Mg^{2+} Interaction. To determine if the above observations about the QM/MM shielding calculations hold more generally, we examined 1′-deoxyribose interacting with a solvated (five water molecules) magnesium ion. The optimized structure at the B3LYP/6-31G(d) level is shown in Figure 7, and the predicted shielding parameters are summarized in Table 4. From the structure, we see that two water molecules bound to Mg^{2+}, labeled W_1 and W_2 in Figure 7, are also involved in a hydrogen bond with the anomeric oxygen O_a and with O_3' in the 1′-deoxyribose, respectively. The hydrogen bond between W_1 and O_a is very strong, reflected by its short distance (1.621 Å). To determine the relative importance of charge transfer and electrostatic effects for the shielding, a series of QM/MM calculations with zero, one (W_1), and two (W_1,W_2) water molecules treated with QM have been carried out as indicated in Table 4. A calculation with a point charge model for Mg^{2+} was also performed. In these QM/MM calculations, the ribose is described by B3LYP.

For QM/MM calculations with all MM water molecules, all ribose shielding parameters are in good agreement with full QM values, except for those of O_2', O_3', and O_a, which are either in close contact with Mg^{2+}, or hydrogen bonded to the water molecules. When W_1 is treated with QM, the shielding of O_a is greatly improved, largely due to the improvement in the electronic distribution around O_a, which is reflected by the change of its Mulliken charge (Figure 7). The shielding of O_2' and O_3' remains in poor agreement with the full QM results. When both W_1 and W_2 are treated with QM, however, all shielding parameters are in excellent agreement with the full QM calculation. The Mulliken charges on O_2' and O_3' change little, which suggests that the improvement in their shielding is mainly due to the inclusion of the Pauli repulsion effect from the QM W_2. It should be noted that the Mulliken charge on the magnesium is still rather large, +1.42, compared to the full QM results of +0.95. If we use a point charge of +2.00 for the Mg^{2+}, but treat W1 and W2 with QM, the obtained QM/MM shielding parameters of all the atoms except O_2' are in good agreement with the full QM results. The O_2' is strongly polarized in this case, as indicated by its largely negative Mulliken charge. Evidently, the charge transfer effect does not have to be completely correct to obtain accurate shielding, if the atoms of interest have reasonable charge. If a point charge of +1.00 is used for Mg^{2+}, the Mulliken charge on O_2' is close to the value

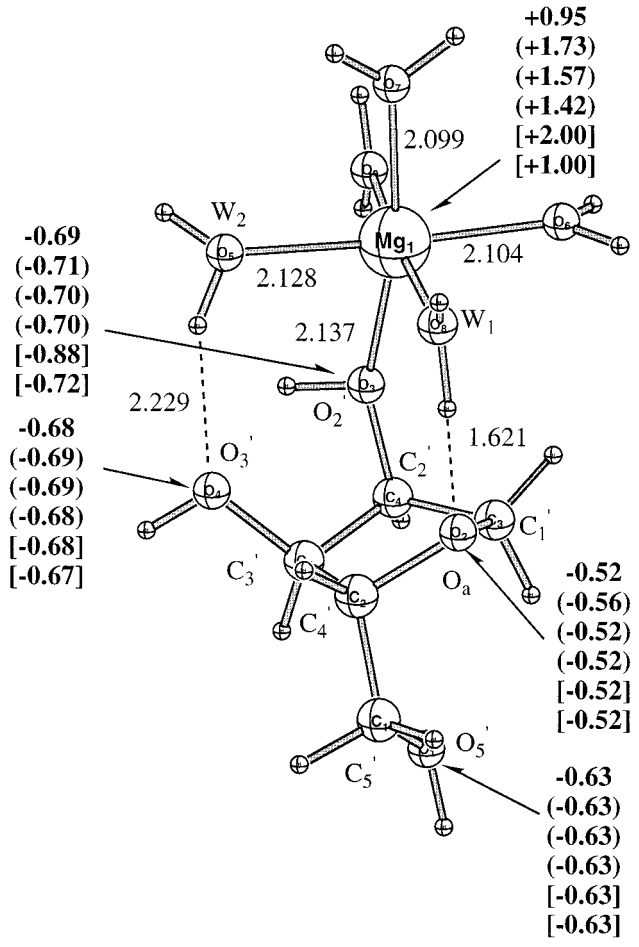

Figure 7. Structure of 1′-deoxyribose interacting with solvated magnesium ion optimized at the B3LYP/6-31G(d) level. The numbers in bold face are Mulliken charges on the magnesium ion at the full QM and QM/MM (numbers in parentheses) levels. The numbers in brackets are Mulliken charges obtained from the "2QM, 3MM, MM Mg" calculations (see Table 4), where the Mg^{2+} is treated as a point charge of +2.00 or +1.00.

from the full QM calculation (Figure 7). Accordingly, the shielding for O_2', 288.2 ppm, is close to the full QM value of 289.5 ppm. The shielding for other atoms, however, are in somewhat worse agreement with the QM values compared to

TABLE 4: Computed Absolute Chemical Shielding Parameters (in ppm) for 1′-Deoxyribose Interacting with Solvated Mg^{2+} [a]

		QM/MM[c]				
atom[b]	full QM	0QM, 5MM	1QM, 4MM	2QM, 3MM	2QM, 3MM, MM Mg	2QM, 0MM
O_a	250.7/90.0	267.8/107.6	251.4/90.9	250.9/90.8	251.8(246.1)/94.0(94.2)	250.5/90.9
C_1'	117.0/56.0	113.9/53.3	116.1/55.2	116.1/55.1	117.3(117.2)/56.9(58.2)	114.9/53.6
C_2'	111.7/38.4	110.2/40.0	111.1/38.9	111.2/38.3	111.8(114.0)/37.6(31.4)	108.8/42.2
O_2'	289.5/67.2	307.2/72.8	304.1/70.0	291.3/72.3	306.3(288.2)/104.2(69.5)	280.8/67.5
C_3'	114.1/40.8	113.8/40.7	114.5/40.0	113.6/40.8	113.8(114.3)/41.4(43.0)	112.5/39.1
O_3'	294.5/44.2	304.4/54.5	302.8/54.6	295.0/43.4	294.4(289.4)/43.0(46.7)	296.4/41.9
C_4'	103.3/40.7	102.6/41.4	103.2/41.9	103.1/41.1	103.2(104.5)/41.3(39.9)	102.7/41.6
C_5'	124.6/35.6	124.2/36.0	124.7/35.9	124.7/35.8	124.6(123.7)/35.8(36.0)	124.9/36.0
O_5'	306.3/104.5	306.1/104.2	306.5/103.8	306.4/103.8	306.3(303.5)/104.2(106.8)	306.7/103.3

[a] For the format of the shielding parameters, see the footnote a of Table 1. [b] For atomic numbering scheme, see Figure 7. [c] In the QM/MM calculations, the 1′-deoxy-ribose and a selected number of water molecules are treated with QM (see text), the rest of the water molecules are treated with the modified TIP3P model. In the "2QM, 3MM, MM Mg" calculation, the Mg^{2+} is treated with a point charge of +2.00 or +1.00 (numbers in parentheses). In the "2QM, 0MM" calculation, W_1, W_2, and Mg^{2+} are treated with QM, and the other water molecules are not included.

the QM/MM results obtained with a point charge of +2.00 for Mg^{2+}.

From the examples in this subsection, we see that to accurately predict shielding of atoms close to the metal ion, ligands of the metal ion have to be treated at the QM level to allow charge transfer. Sometimes satisfactory shielding values can be obtained even when the charge transfer effect is not fully described, if the atom of interest has an appropriate Mulliken charge. Since the effect from Pauli repulsion is rather important at short distances, an MM description is usually not adequate for molecules forming hydrogen bonds with the atoms of interest. For atoms more than 2.5 Å from the metal ions and its ligands, an MM description of the metal environment, or even the ion itself, is sufficient to derive rather accurate chemical shielding parameters; in some cases the contributions are as large as 20 ppm.

III.5. Model for Liganded Myoglobin. Myoglobin is a protein for which extensive chemical shift data concerning the binding site exist. McMahon et al.[77] have carried out a series of experimental as well as theoretical investigations of chemical shifts in model systems that mimic myoglobin (Mb). They examined the effect of ligand (CO) bending and tilting on the ^{57}Fe, ^{13}C, and ^{17}O chemical shifts but they have not explicitly considered the environment. Here, we present results for a simplified Mb·CO model that includes the distal histidine, and has been used in illustrating QM/MM vibrational calculations.[33] Three structures are considered, as shown in Figure 8. The first structure, referred as **com_i**, is an isolated model heme−CO complex, which is calculated with full QM. The two other structures, referred as **com_h1** and **com_h2**, respectively, includes an imidazole that represents the distal histidine in two different orientation, which correspond to two substates of myoglobin.[81] The three systems have been calculated with full QM and with the QM/MM method. In the QM/MM treatment, the QM system consists of the model heme and CO, and the imidazole is described by the CHARMM22 force field.[78] The QM calculations are performed with B3LYP. The basis set used in the geometry optimization is the double-ζ set from Ahlrichs and co-workers.[79] In the chemical shielding calculation, a larger all electron (9s5p2d) basis set is used for Fe, and the 6-31G-(d,p) basis is used for the main group elements. To avoid large changes in the relative orientation of the imidazole and model heme in **com_h2**, the position of the Fe, and that of the CE1, HE1 atoms of imidazole are fixed during geometry optimization.

The optimized structures are shown in Figure 8, in comparison with the data from recent high-resolution X-ray study.[80] The effect of the distal histidine on the CO-heme geometry is not large, and is well reproduced at the QM/MM level. The chemical shielding is tabulated in Table 5. Upon binding of the imidazole in **com_h1**, the isotropic shielding and the CSA of Fe and O undergo significant changes; the effect on the carbon in CO is smaller. In **com_h2**, the shielding of Fe and C change in the directions opposite to that in **com_h1**. Part of the difference between the two species originates from the Fe−C bond lengths, which are 1.747 and 1.783 Å in **com_h1** and **com_h2**, respectively. Comparing the full QM and the "no MM" results in Table 5, which are obtained at the optimized **com_h1**/**com_h2** geometries excluding the effect of the imidazole, it is clear that the influence from the imidazole on the model heme is more significant in **com_h1**. This is expected since the imidazole is much closer to the model heme−CO moiety in that case. We also note that the difference between the ^{13}C shielding in the two species is of opposite sign from that of ^{17}O; this is in agreement with the previous study of the electric field effects on CO chemical shifts.[81] In the study of McMahon et al.,[77] a number of spectroscopic data and DFT calculations on model heme−CO compounds were used to determine the orientation of CO in a series of heme proteins. The effect of the histidine on the chemical shift, which was not included by them, is significant according to the present calculations. However, further analysis is required to determine whether it alters their conclusions.

The QM/MM calculations are in fair agreement with the full QM results for both **com_h1** and **com_h2**, especially if the full QM geometry is used. Most importantly, the differences in the chemical shielding of the two species given by the QM/MM calculations are very similar to the full QM results. Thus, in this case the QM/MM calculation has the accuracy required for distinguishing different conformers.

III.6. 1-N Chemical Shielding in NAD^+. Previous studies have shown that MP2 calculations tend to give more accurate chemical shielding results than DFT with a current-independent exchange correlation functional.[6,17] However, the expense of such calculations at the MP2 level is very high. It has been estimated that on a standard workstation computer, one can afford systems with up to 200 basis functions if no symmetry is present.[11] A recent integral-direct implementation has extended the limit to about 400 basis functions.[82] Nevertheless, MP2 shielding calculations remain prohibitive for larger molecules. This makes the QM/MM approach particularly important for performing MP2 shielding calculations for only one part of a large molecule.

We illustrate this possibility by calculating the shielding for the 1-N atom in nicotinamide adenine dinucleotide (NAD^+), an important redox coenzyme. It has been shown experimentally[83] that the shielding of 1-N in NAD^+ is downfield by 16−

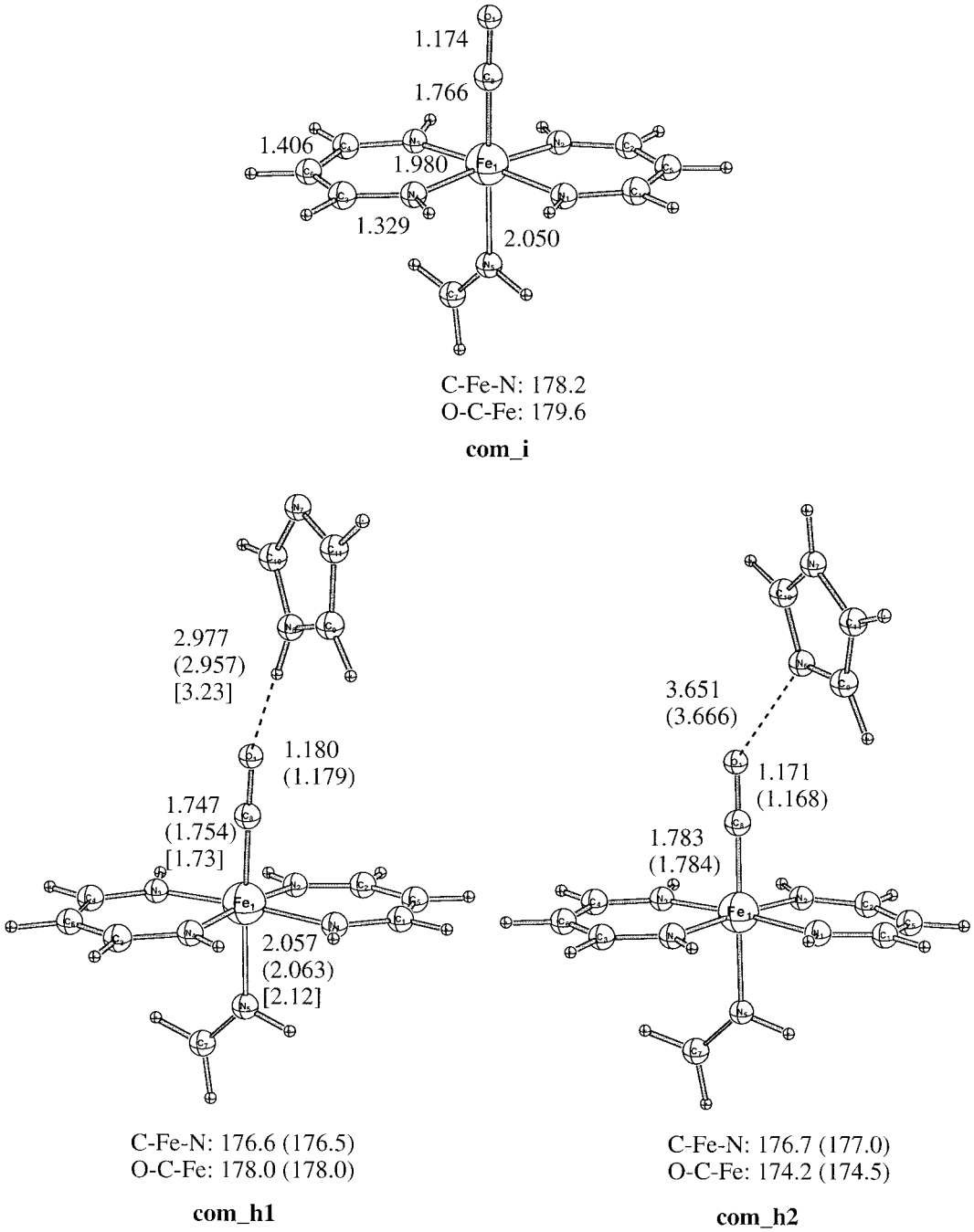

Figure 8. Structures of simple models for myoglobin−CO optimized with the QM and QM/MM method (numbers in parentheses). The numbers in brackets are from a high-resolution X-ray structure of Mb·CO (ref 80). In the QM/MM calculation, the model heme−CO complex is described with B3LYP, and the model distal histidine (imidazole) is treated with CHARMM22 force field. The basis set used in the geometry optimization is the double-ζ set from Ahlrichs and co-workers (ref 79). In the chemical shielding calculation, a larger all-electron (9s5p2d) basis set is used for Fe and the 6-31G(d,p) basis is used for the main group elements.

17 ppm, depending on the solvent and pH values, relative to the *N*-methyl nicotinamide. The effect has been rationalized in terms of the electron withdrawing character of the ribose moiety of NAD^+.[83] We examine the role of the ribose in the present QM/MM calculation. The structure of *N*-methyl nicotinamide was optimized at the level of B3LYP/6-31G(d). The structure of NAD^+ was optimized with the QM/MM method starting with the geometry taken from the X-ray structure of NAD^+ bound to the horse liver alcohol dehydrogenase.[84] The QM/MM partition used for the calculation is indicated in Figure 9. The QM part corresponds to *N*-methyl nicotinamide, which is treated with B3LYP/6-31G(d). The MM parameters are from the CHARMM22 force field for nucleic acids.[60] The shielding calculations have been carried out at both the B3LYP and MP2 level, with the 6-31G(d) basis set. Calculations at the B3LYP level with a larger 6-311+G(d) basis set have also been performed to confirm the smaller basis set results.

The geometries of NAD^+ and *N*-methyl nicotinamide are quite similar, as expected (Figure 9), with the largest difference about 0.02 Å in bond length. The computed shielding for 1-N in *N*-methyl nicotinamide with NH_3 as the reference, are 194.8, 196.0, and 222.7 ppm, at the B3LYP/6-31G(d), MP2/6-31G(d), and B3LYP/6-311+G(d) level, respectively. These deviate substantially from the experimental value of ~209.0 ppm. Part of the error is likely to originate from the neglect of the solvent effect. For MP2, the small size of the basis set may also

TABLE 5: Computed Absolute Chemical Shielding Parameters (in ppm) of a Model for Myoglobin (Mb)−CO[a]

		com_h1			
atom[b]	**com_i**	full QM	QM/MM[c]	QM/MM opt[d]	no MM[e]
^{57}Fe	−10117.5/3213.5	−9643.0/3151.7	−9701.0/3171.8	−9839.4/3159.8	−9827.1/3212.6
^{13}C	−61.3/479.5	−64.1/492.3	−63.6/486.4	−63.9/488.1	−64.7/478.7
^{17}O	−109.2/926.9	−82.8/892.4	−90.3/899.5	−92.8/904.0	−113.7/928.1

	com_h2			
	full QM	QM/MM[c]	QM/MM opt[d]	no MM[e]
^{57}Fe	−10383.4/3258.9	−10412.9/3268.1	−10458.7/3289.3	−10329.8/3240.6
^{13}C	−56.8/472.6	−56.6/470.8	−56.0/469.0	−56.9/478.0
^{17}O	−108.9/928.2	−111.4/929.8	−109.8/925.5	−101.3/923.2

[a] The QM level here is B3LYP. The basis set used in the geometry optimization is the double-ζ set from Ahlrichs and co-workers.[79] In the chemical shielding calculation, a larger all-electron (9s5p2d) basis set is used for Fe, and the 6-31G(d,p) basis is used for the main group elements. For comparison, the shielding for C and O in free CO are, 2.8/403.7 ppm and −64.7/710.9 ppm, respectively. For the format of the shielding parameters, see footnote a of Table 1. [b] The atoms are the iron atom in the model heme and the carbon and oxygen atoms in the carbon monoxide bound to the iron. [c] The QM/MM chemical shielding tensors at the full QM geometry. In the QM/MM calculations, the imidazole is described by the CHARMM22 force field. [d] The QM/MM chemical shielding tensors at the QM/MM optimized geometry. [e] The imidazole is not included in the calculation. The geometry of the model heme-CO is that in the full QM **com_h**.

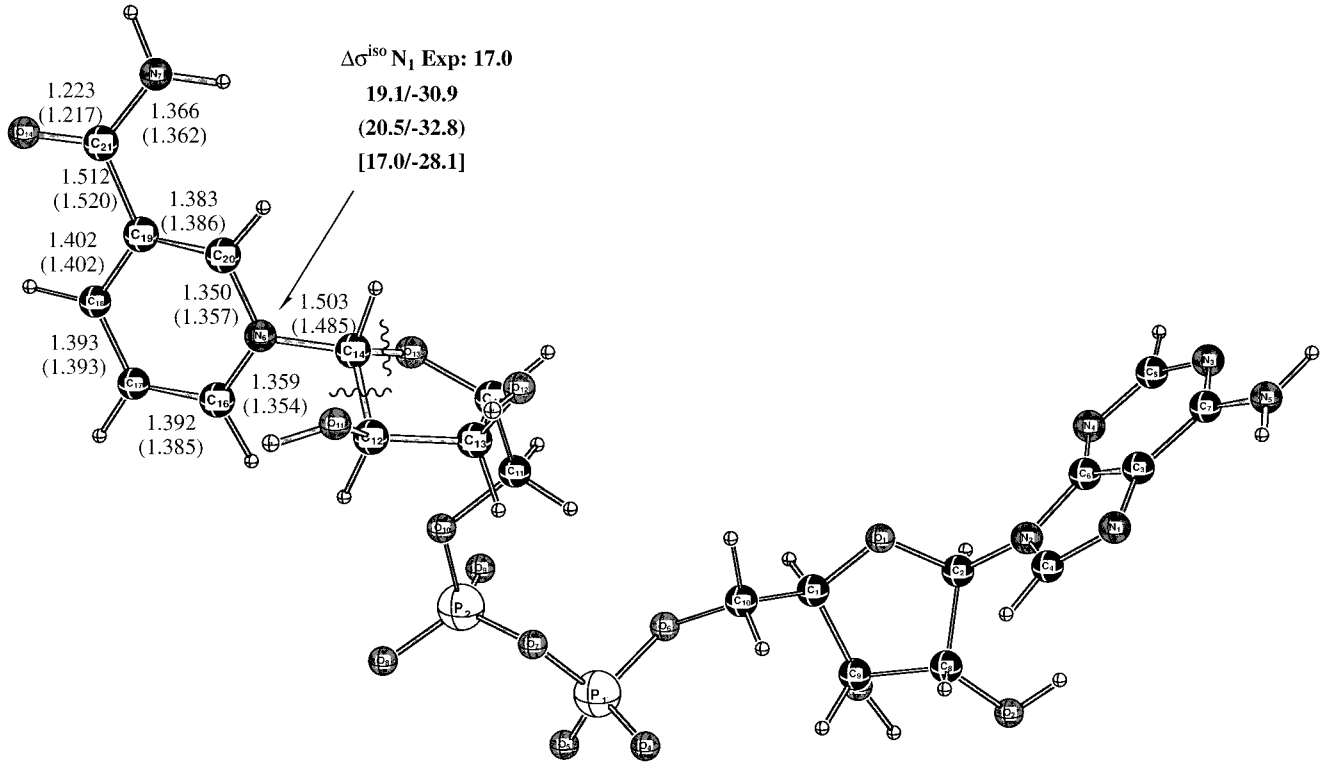

Figure 9. Geometry and chemical shielding for NAD^+ (nicotinamide adenine dinucleotide, reduced form). The geometry for NAD^+ is optimized with the QM/MM method with the partition indicated by the wavy lines the figure. The values in the parentheses are geometrical parameters for the *N*-methyl nictoniamide, optimized at the B3LYP/6-31G(d,p) level. The bold numbers are the relative chemical shielding for the 1-N atom in NAD^+ compared to *N*-methyl nicotinamide, calculated with the QM/MM approach. The numbers are obtained with the B3LYP/6-31G(d); the numbers in parentheses are calculated with the B3LYP/6-311+G(d,p); and the numbers in brackets are computed with the MP2/6-31G(d) method. The numbers before the slashes are the isotropic components, and these after the slashes are the anisotropies.

introduce some error. The sugar pucker conformation of the ribose may also influence the shielding of N_1, although the magnitude of the effect should be smaller than that on the ribosyl carbon atoms found in previous studies.[25,85] The *relative* shielding for the 1-N in NAD^+ and *N*-methyl nicotinamide, however, are well reproduced by all the methods used. The calculated values are 19.1, 20.5, and 17.0 ppm at the B3LYP/6-31G(d), B3LYP/6-311+G(d), and MP2/6-31G(d) level, respectively, compared to the experimental value of 16−17 ppm. In this case, the relative values are not very sensitive to the size of the basis set, which justifies the use of small basis set with MP2. The excellent agreement between the MP2 result and the experimental value certainly is fortuitous, since no solvent corrections have been included. Nevertheless, this example illustrates that one can obtain useful results with the MP2/MM approach for large molecules that cannot be treated as a whole with the MP2 method, though in the present case the MP2 correction is small.

III.7. Solvent Effect on Chemical Shielding. The effect of solvation on chemical shielding is of great importance because most reactions of interest occur in solution. Several continuum dielectric models have been used, and qualitatively correct results were obtained for small solute molecules including water,[86] CH_3CN, and CH_3NO_2.[39]

As an example of the QM/MM approach, we study the solvent effect on the shielding of water. The problem has been

investigated by a number of authors. Malkin et al.[87a] and Chesnut et al.[87b] calculated the chemical shift of liquid water relative to the gas phase with the supermolecule/MD approach. The results were found to depend rather sensitively on the force field used in the MD simulations, and values ranging from −20 (with the CFF-91 force field in Discover[87(a)]) to −47 ppm (with the potential developed by Bopp, Jancsò and Heinzinger[88]) were obtained for the O^{17} chemical shift. Empirical approaches have also been applied to the same problem, although the results are considerably worse. [89]

In the present calculations, we carried out molecular dynamics at 300 K for a 16 Å water sphere with a deformable stochastic boundary potential.[90] Water molecules beyond 12 Å from the center of the sphere were treated with Langevian dynamics (LD), while Newtonian dynamics (MD) was used for the molecules in the interior. The LD/MD division was updated every 25 steps to take account of the water molecules that move across the boundary. Two water potentials were tested. The first one is the standard rigid TIP3P model,[54] and the second is the flexible TIP3P model developed by Pettitt et al.[91] A time step of 2 fs was used in the simulation with the rigid TIP3P model, and a value of 0.2 fs was used with the flexible water model. The system was first equilibrated starting from 100 to 300 K for 10 ps, and the production run was then carried out for another 10 ps. QM/MM calculations were carried out for 100 snapshots separated by 50 integration steps. The QM region included the central "solute" water molecule plus the "solvent" water molecules within 3 Å. This usually gives a cluster size of 7 to 8 and includes all the water molecules directly hydrogen bonded to the one of interest. Water molecules within 10 Å of the "solute" are included as the MM part. A number of test calculations without the MM part indicated that the MM contribution is about 5 ppm for the oxygen and 0.5 ppm for the hydrogen atoms. The QM level is B3LYP/6-311G(d,p), and counterpoise (CP) corrections were included by computing the chemical shift of the central water in the presence of basis functions on the other QM atoms. Test calculations with a larger basis set (6-311++G(d,p)) for 10 configurations from the trajectory with the rigid TIP3P model showed that the B3LYP/6-311G(d,p) approach with CP correction gives reasonable, though approximate, shielding for water in the cluster relative to the water monomer; typical errors are 7 ppm for the oxygen and 0.5 ppm for the hydrogen atoms.

The O−O radial distribution functions, $g_{OO}(r)$, computed using 40, 100, and 250 configurations are presented in Figure 10. During the calculation of $g_{OO}(r)$, only the pairs including the oxygen atom in the central water were counted to avoid effects due to the boundary condition. The distribution of isotropic shifts and CSA calculated for the 100 snapshots are plotted in Figure 11. The autocorrelation functions of the isotropic and anisotropic shifts for the oxygen and hydrogen atoms are shown in Figure 12. The cross-correlation functions for the oxygen−hydrogen shifts are also plotted. For the correlation functions involving hydrogen atoms, the average values for the two hydrogen atoms in the central water molecule are presented. The O−O radial distribution functions in Figure 10 are in reasonable agreement with previous theoretical studies[91,92] and experimental measurements.[93] The height of the first peak in $g_{OO}(r)$ obtained with the rigid TIP3P model is somewhat higher than that obtained with the flexible TIP3P model. Oscillatory behavior is observed in $g_{OO}(r)$ at distances larger than 4 Å, which is likely to be due to the limited number of configurations (<250) sampled in the calculations. However, it is seen that the structure of $g_{OO}(r)$ at distances less than 4 Å

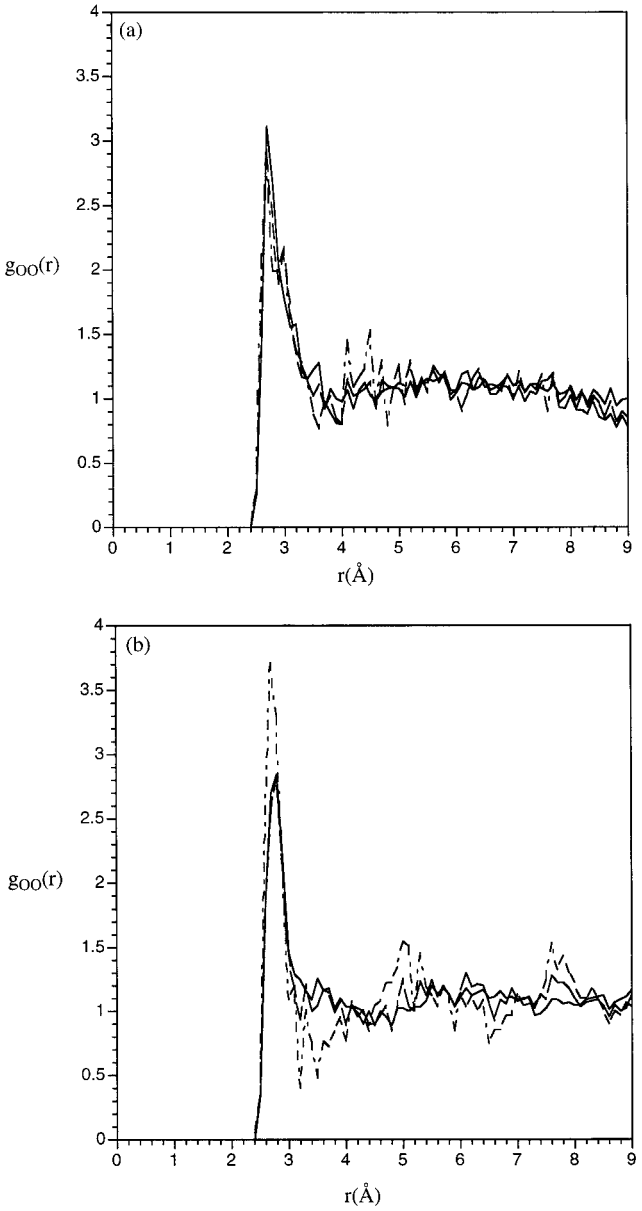

Figure 10. The oxygen−oxygen pair distribution function, $g_{OO}(r)$, calculated with 40 (point dash), 100 (dash), and 250 (solid) configurations from the molecular dynamics calculations. The plot in (a) was obtained with the rigid TIP3P model, and (b) was obtained with the flexible TIP3P model of Dang and Pettitt (ref 91).

has converged, even when only 100 configurations are used. This suggests that using 100 configurations in the NMR calculations should be sufficient.

The results from the rigid and flexible TIP3P models are rather close, especially for the hydrogen atoms. The isotropic shifts for the oxygen atom differ somewhat more; they are −27.6 and −22.3 ppm with the rigid and flexible water model, respectively. The range of the chemical shifts found in the different configurations are rather large using either water model (see Figure 11); they vary from −60 to 10 ppm and from −40 to 30 ppm, for the isotropic and anisotropic shielding of the oxygen atom, respectively. On average, the shift in the oxygen CSA is rather small, −3.2 and 0.2 ppm, using the flexible and rigid water model, respectively. For the hydrogen atoms, the isotropic shift ranges from −7 to 1 ppm, and the anisotropies lie between −5 to 25 ppm. The average values for the two quantities are −2.9 and 7.7 ppm, respectively, with the flexible

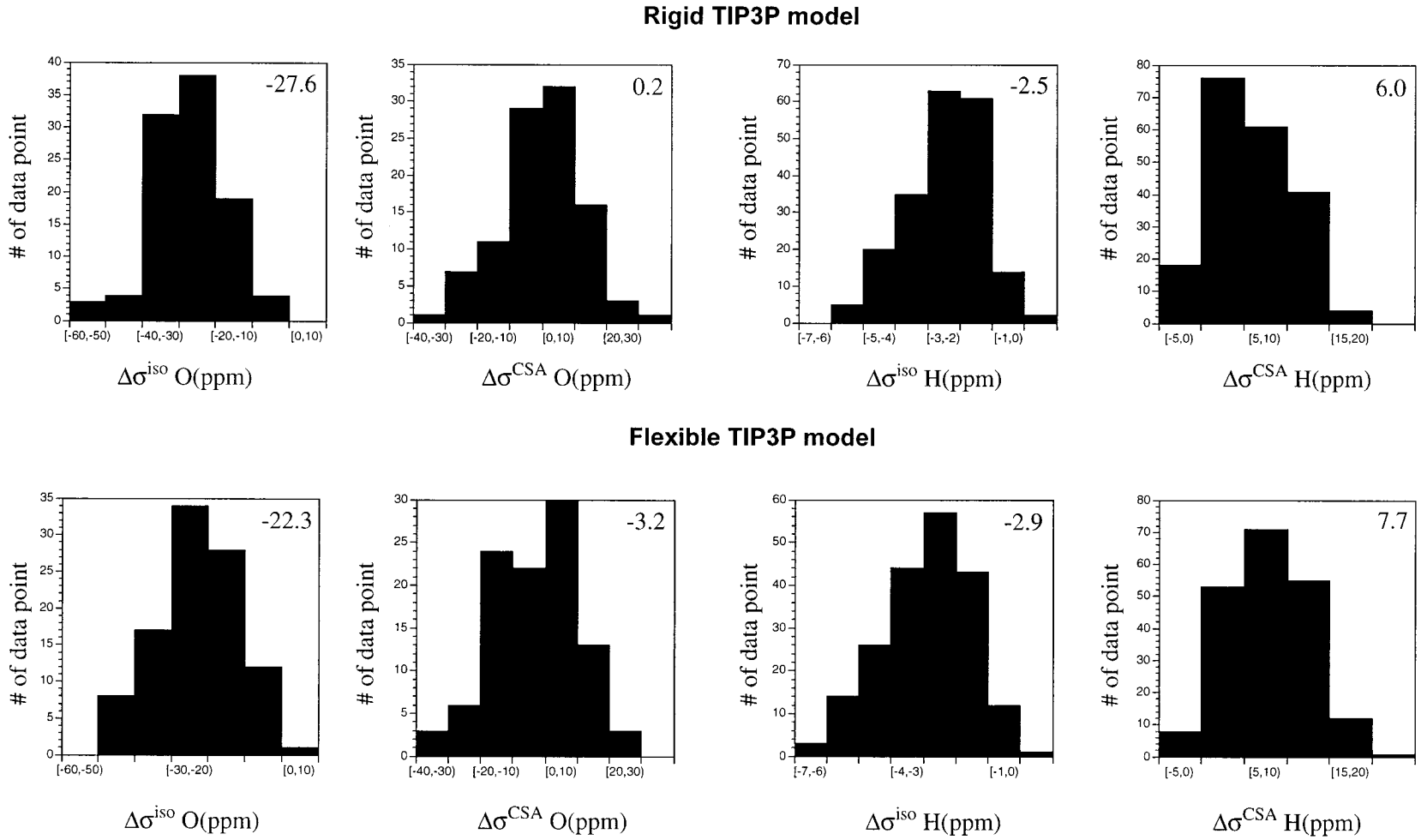

Figure 11. Distributions of chemical shielding of oxygen and hydrogen atoms in the central water molecule in a 16 Å water sphere. The chemical shielding parameters are calculated relative to the tagged water molecule in the presence of the basis functions on the water molecules within 3.0 Å, which are also treated quantum mechanically. Note that there are twice as many data points for the hydrogen atoms than oxygen because there are two hydrogen atoms in a water molecule. The first and second row data are obtained with 100 configurations from molecular dynamics using the rigid and flexible TIP3P model, respectively. The numbers in the upper right corner of the plots are the average values.

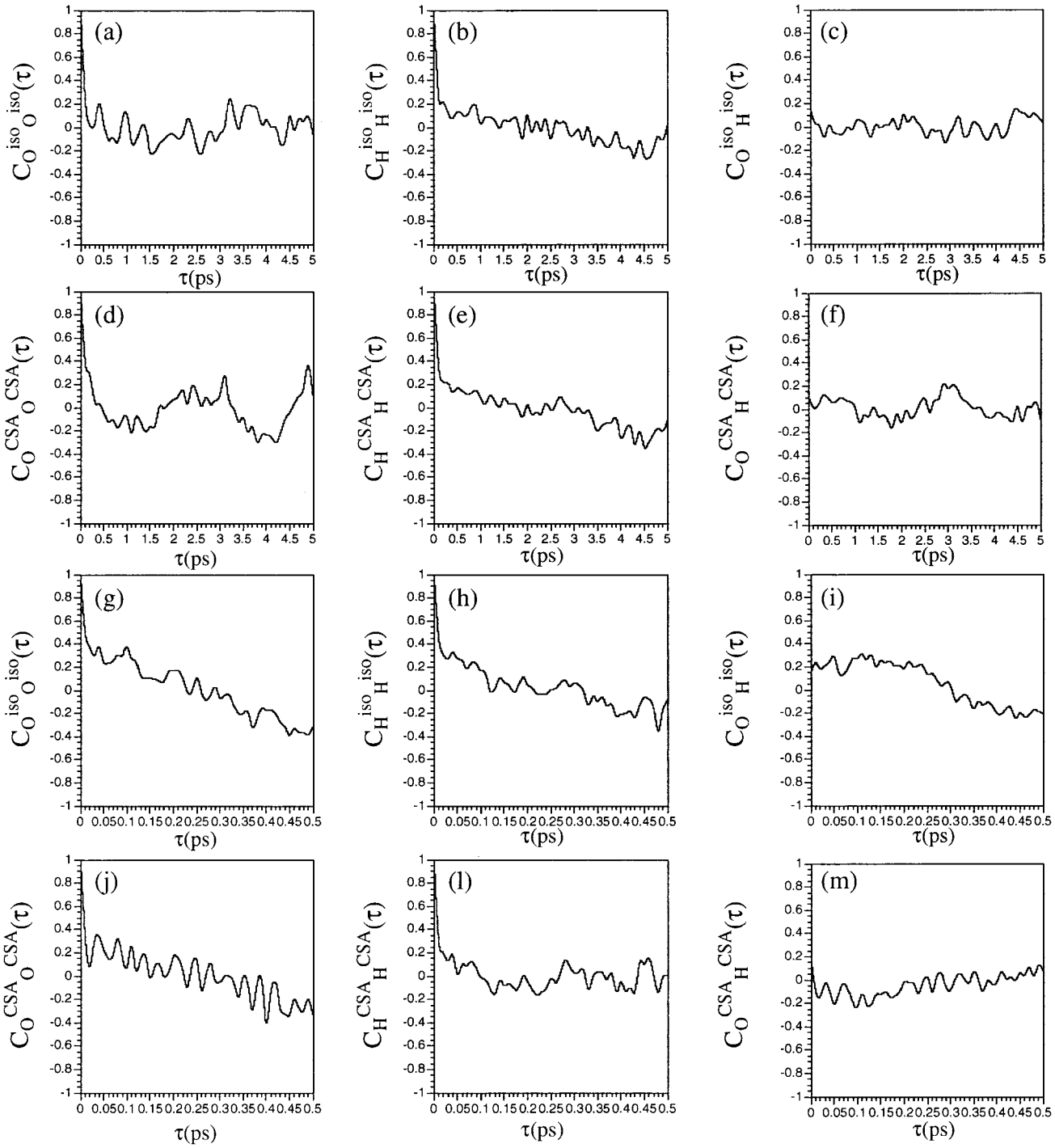

Figure 12. Autocorrelation and cross-correlation functions of the isotropic shifts and CSA for the oxygen and hydrogen atoms in liquid water. For the correlation functions involving hydrogen, the average results for the two hydrogen atoms in the central water molecule were considered. Plots a−f were obtained with the rigid TIP3P model, and (g−m) were obtained with the flexible TIP3P model of Dang and Pettitt (ref 91).

TIP3P model; the corresponding values are −2.5 and 6.0 ppm, respectively, with the rigid TIP3P model.

There is noise in the computed correlation functions (Figure 12), because of the small number of configurations. Nevertheless, several qualitative features are evident. First, the initial decays of the autocorrelation functions of the isotropic shifts are very fast for both the oxygen and hydrogen atoms; they are on the order of 0.05 ps. The same applies to the CSA autocorrelation functions. There is some structure in all the autocorrelation functions, obtained with both the flexible and rigid water potentials. In the case of oxygen CSA autocorrelation function with the flexible TIP3P model, the fast oscillation appears rather regular. The corresponding autocorrelation function with the rigid TIP3P model, by contrast, shows less regular structure. This suggests that the internal vibration of the water molecule have considerable influence on the CSA of the oxygen atom. The effect is reduced by averaging over large number of configurations, as indicated by the similar values of the mean oxygen CSA, −3.2 and 0.2 ppm, obtained with the flexible and rigid water potential, respectively. There is little cross-correlation between the oxygen and hydrogen shifts, suggested by the relatively small values ($\sim$ 0.2) of the cross-correlation functions in Figure 12. Clearly, the results shown here are only indicative and longer simulations would be required to

obtain definitive results. Such calculations are possible with the QM/MM model.

The results obtained here can be compared with the values calculated in a supermolecule study by Malkin et al.[87a] Molecular dynamics were carried out at both the gas-phase and the liquid-phase density. From those trajectories, 40 water clusters of size 9 and 10 clusters of size 13 were then collected, and chemical shift calculations were performed with the SOS-DFPT approach using the IGLO-III basis set.[8] The results were found to be rather sensitive to the water potential used in the MD calculations. With the water potential from Lie and Clementi,[94] the chemical shift from gas to the liquid water was found to be −36.8 ppm for the oxygen and −3.4 ppm for the hydrogen atoms. The chemical shift for the oxygen obtained with two empirical potentials for the water molecular dynamics, developed by Bopp, Jancsò, and Heinzinger[88] and by Dang and Pettitt[91] (the same as used in the present calculation), respectively, is larger in magnitude by 9.8 and 8.0 ppm, respectively. The results obtained with the Lie−Clementi potential are in surprising agreement with the experimental values[95] of −36.1 and −4.3 ppm, respectively, since the contribution of more distant water molecules was neglected. As mentioned above, the contribution from water molecules beyond cluster of size 8 is about 5 ppm for the oxygen shift and 0.5 ppm for the hydrogen shift. The shifts were further decomposed into "intra" and "inter" molecular contributions by Malkin and co-workers.[87a] The former is obtained by comparing the shielding of a water monomer from the liquid- and gas-phase MD trajectory, respectively. This term arises from the difference in the vibrational motion of water in the liquid and gas phase. The intermolecular part is the difference between the shielding of the water in clusters and the water monomer, both configurations taken from liquid MD trajectory. This term was found by Malkin et al.[87a] to be −30.4 ppm for the oxygen and −2.7 ppm for the hydrogen atoms with the Lie−Clementi water potential; the corresponding values are −37.3 and −2.5 ppm with the Dang−Pettitt potential. The present calculations considered only the intermolecular component, and the results are −22.3 and −2.9 ppm for oxygen and hydrogen, respectively, with the Dang−Pettitt flexible water potential. Considering the typical error of 7 ppm for the oxygen and 0.5 ppm for the hydrogen with the B3LYP/6-311G(d,p) approach compared with B3LYP/6-311++G(d,p), observed for 10 configurations from the trajectory with the rigid TIP3P model as mentioned above, our results are in fair agreement with the results of Malkin et al.[87a] Indeed, with these 10 configurations, the B3LYP/6-311++G(d,p) gives −32.0 ppm for the oxygen shift and −2.8 ppm for the hydrogen shift. The shift in the CSA is −7.0 and 4.6 ppm for the oxygen and hydrogen, respectively.[87a] The remainder of the differences, around 5 ppm for the oxygen shift, are likely to be due to the fact that long-range contributions were neglected in the work of Malkin and co-workers.[87a] Furthermore, it is seen that $g_{OO}(r)$ is not well converged even at short distances if only 40 configurations are considered (Figure 10). Therefore, limited sampling of configurations in the study of Malkin et al.[87a] may also introduce some errors in the computed chemical shifts.

We have demonstrated that one may use the QM/MM-MD approach to study the solvation effect on chemical shielding. The merit of the QM/MM method compared to the pure QM cluster approach is that long-range solvation effect, which typically amount to several ppm, can be included. In addition, smaller numbers of solvent molecules have to be treated with QM in the QM/MM approach, so that sampling of a larger number of solvent configurations is possible. To obtain an accurate result, high-level calculations have to be used for the QM part of the system.

IV. Conclusion

Combined quantum mechanical/molecular mechanical (QM/MM) methods have been shown to be powerful tools for studying the properties of macromolecular systems in which the electron distribution plays a direct role. Examples are enzyme catalysis and covalent ligand binding. We have extended the QM/MM methodology to compute molecular properties based on analytical derivatives. The first paper of the series dealt with vibrational calculations.[33] In the present paper, we implemented QM/MM calculations of chemical shifts. The current implementation makes it possible to compute shielding parameters *consistent* with the geometry obtained at the same level and as part of a molecular dynamics simulation for properties, such as NMR relaxation due to the chemical shift anisotropy.

Test calculations for a range of systems have demonstrated that QM/MM method with an appropriate QM/MM partition offers a good description of the environmental effects on chemical shifts. Typical errors relative to full QM calculations with the same basis set are about 1−2 ppm for heavy atoms at distances greater than 2.5 Å. At shorter distances (e.g., those involved in hydrogen bonding), significant deviations from the full QM results are observed since neither the Pauli repulsion nor the magnetic susceptibility of the environment is considered in the present QM/MM model. A straightforward approach to correct this is to extend the QM region to include all the ligands that interact directly with the atom of interest. This was illustrated with the example of 1′-deoxyribose interacting with a solvated magnesium ion. The one-electron effective operator approach that has been adopted in the EFP[49] method may be another alternative. An advantage of using QM/MM to describe environmental effect is that BSSE can be avoided; this can be significant for oxygen when a medium size basis set is used.

The shieldings of the base atoms in CMP and in paired and stacked bases are well described with the QM/MM method. This shows the potential of the QM/MM method in obtaining structural information for nucleic acids. To predict accurately the chemical shielding for atoms close to a metal ion, the QM description of the metal ion environment must take account of the charge transfer effect between the metal and its ligands. However, for atoms reasonably far (>2.5 Å) from the metal and its ligands, the MM description of the environment appears to be adequate even when polarization effects are substantial. For the myoglobin−CO model, it is found that the distal histidine has significant influence on the shielding of Fe and CO, and the effect is well reproduced at the QM/MM level. With NAD^+ as an example, we illustrated that MP2/MM can be used to compute accurate shielding for atoms in large molecules that cannot be treated with pure MP2. Finally, we have used the QM/MM-MD approach to study the solvation effect on the shielding of water. The results are in only fair agreement with previous studies with pure QM clusters and experimental measurements unless a large basis set is used.

The purpose of this paper has been to demonstrate the feasibility of the QM/MM method for the calculation of shielding parameters in macromolecular systems. Applications to problems of specific interest are in progress.

Acknowledgment. We thank F. Leclerc for many interesting discussions on NMR related issues in nucleic acid systems. Discussions with M. Buck, A. Dejaegere, and H. Guo are also appreciated. The work was supported in part by a grant from

the Department of Energy. Part of the calculations have been performed on the CRAY J90 machines as well as CRAY T3E machines at NERSC and IBM SP2 at CCST of the Argonne National Lab.

References and Notes

(1) See, for example: (a) Grant, D. M.; Harris, R. K., Eds. *Encyclopedia of nuclear magnetic resonance*; Wiley: New York, 1996. (b) Wüthrich, K. *NMR in structural biology*; World Scientific: Singapore, 1995. (c) Brooks, C. L., III; Karplus, M.; Pettitt, B. M. *Proteins: A Theoretical Perspective of Dynamics, Structure, & Thermodynamics;* Adv. Chem. Phys. LXXI; John Wiley & Sons: New York, 1988.

(2) See, for example: (a) Ösapay, K.; Case, D. A. *J. Biomol. NMR* **1994**, *4*, 215. (b) Case, D. A.; Dyson, H. J.; Wright, P. E. *Methods Enzymol*. **1994**, *239*, 392. (c) Case, D. A. In *Encyclopedia of Computational Chemistry*; John Wiley: New York, 1998. (d) Sitkoff, D.; Case, D. A. *Prog. NMR Spectrosc*. **1998**, *32*, 165. (e) deDios, A. C.; Pearson, J. G.; Oldfield, E. *Science* **1993**, *260*, 1491. (f) Le, H.; Oldfield, E. *J. Biomol. NMR* **1994**, *4*, 341. (g) Halvin, R. H.; Le, H.; Laws, D. D.; deDios, A. C.; Oldfield, E. *J. Am. Chem. Soc*. **1997**, *119*, 11951. (h) Wishart, D. S.; Sykes, B. D.; Richards, F. M. *J. Mol. Biol*. **1991**, *222*, 311.

(3) See, for example: (a) Ösapay, K.; Theriault, Y.; Wright, P. E.; Case, D. A. *J. Mol. Biol*. **1994**, *244*, 183. (b) Botuyan, M. V.; Toy-Palmer, A.; Chung, J.; Blake, R. C., II; Case, D. A.; Dyson, H. J. *J. Mol. Biol*. **1996**, *263*, 752.

(4) (a) Ramsey, N. F. *Phys. Rev*. **1950**, *78*, 699. (b) Ramsey, N. F. *Phys. Rev*. **1953**, *91*, 303.

(5) Kolker, H. J.; Karplus, M. *J. Chem. Phys.* **1964**, *41*, 1259.

(6) (a) Helgaker, T.; Jaszunski, M.; Rudd, K. *Chem. Rev.* **1999**, *99*, 293. (b) Malkin, V. G.; Malkina, O. L.; Eriksson, L. A.; Salahub, D. R. In *Modern Density Functional Theory: A Tool for Chemistry*; Seminario, J. M., Politzer, P., Eds.; Elsevier Science B. V.: New York, 1995.

(7) (a) Ditchfield, R. *Mol. Phys*. **1974**, *27*, 789. (b) Wolinski, K.; Hinton, J. F.; Pulay, P. *J. Am. Chem. Soc*. **1990**, *112*, 8251.

(8) Kutzelnigg, W.; Fleischer, U.; Schindler, M. In *NMR−Basic Principles and Progress*; Springer: Heidelberg, 1990; Vol. 28, p 1965.

(9) (a) Hansen, A. E.; Bouman, T. D. *J. Chem. Phys.* **1985**, *82*, 5035. (b) Hansen, P. E.; Abildgaard, J.; Hansen, A. E. *Chem. Phys. Lett.* **1994**, *224*, 275.

(10) Stanton, J. F.; Gauss, J.; Siehl, H. U. *Chem. Phys. Lett*. **1996**, *262*, 183.

(11) Gauss, J. *J. Chem. Phys.* **1993**, *99*, 3629.

(12) (a) Gauss, J.; Stanton, J. F. *J. Chem. Phys*. **1996**, *104*, 2574. (b) Gauss, J.; Stanton, J. F. *J. Chem. Phys*. **1995**, *102*, 251.

(13) See, for example: Parr, R. G.; Yang, W. *Density-Functional Theory of Atoms and Molecules*; Oxford University Press: New York, 1989.

(14) (a) Vignale, G.; Rasolt, M. *Phys. Rev. Lett*. **1987**, *59*, 2360. (b) Vignale, G.; Rasolt, M. *Phys. Rev. B* **1988**, *37*, 10685. (c) Vignale, G.; Rasolt, M.; Geldart, D. J. W. *Phys. Rev. B* **1988**, *37*, 2502.

(15) (a) van Wüllen, C. *J. Chem. Phys*. **1995**, *102*, 2806 (b) Salsbury, F. R., Jr.; Harris, R. A. *J. Chem. Phys*. **1997**, *107*, 7350.

(16) Lee, A. M.; Handy, N. C.; Colwell, S. M. *J. Chem. Phys*. **1995**, *103*, 10095.

(17) Cheeseman, J. R.; Trucks, G. W.; Keith, T. A.; Frisch, M. J. *J. Chem. Phys*. **1996**, *104*, 5497.

(18) Olsson, L.; Cremer, D. *J. Chem. Phys*. **1996**, *105*, 8995.

(19) (a) Malkin, V. G.; Malkina, O. L.; Salahub, D. R. *Chem. Phys. Lett*. **1996**, *261*, 335. (b) Vaara, J.; Ruud, K.; Vahtras, O.; Ågren, H.; Jokisaari, J. *J. Chem. Phys*. **1998**, *109*, 1212. (c) Nakatsuji, H.; Takashima, H.; Hada, M. *Chem. Phys. Lett*. **1995**, *233*, 95.

(20) Sieber, S.; Schleyer, P. v. R.; Gauss, J. *J. Am. Chem. Soc*. **1993**, *115*, 6987.

(21) Ruiz-Morales, Y.; Ziegler, T. *J. Phys. Chem.* **1998**, *102*, 3970.

(22) Valerio, G.; Goursot, A.; Vetrivel, R.; Malkina, G.; Malkin, V.; Salahub, D. R. *J. Am. Chem. Soc*. **1998**, *120*, 11426.

(23) Salzmann, R.; Kaupp, M.; Mcmahon, M. T.; Oldfield, E. *J. Am. Chem. Soc*. **1998**, *120*, 4771.

(24) Sapay, K.; Theriault, Y.; Wright, P. E.; Case, D. A. *J. Mol. Biol*. **1994**, *244*, 183.

(25) Giessner-Prettre, C.; Pullman, B. *Q. Rev. Biophys*. **1987**, *20*, 113.

(26) (a) Ösapay, K.; Case, D. A. *J. Am. Chem. Soc*. **1991**, *113*, 9436. (b) Wijmenga, S. S.; Kruithof, M.; Hilbers, C. W. *J. Biol. NMR* **1997**, *10*, 337. (c) Williamson, M. P.; Asakura, T. *J. Magn. Reson. B* **1993**, *101*, 63.

(27) Buckingham, A. D.; Schaefer, T.; Schneider, W. G. *J. Chem. Phys*. **1960**, *32*, 1227.

(28) Sternberg, J.; Priess, W. *J. Magn. Reson*. **1997**, *124*, 8.

(29) McConnell, H. M. *J. Chem. Phys*. **1957**, *27*, 226.

(30) (a) Stephen, M. *J. Mol. Phys*. **1958**, *1*, 223. (b) Jameson, C. J.; de Dios, A. C. *J. Chem. Phys.* **1992**, *97*, 417.

(31) Sitkoff, D.; Case, D. A. *J. Am. Chem. Soc*. **1997**, *119*, 12262.

(32) (a) Warshel, A.; Karplus, M. *J. Am. Chem. Soc*. **1972**, *94*, 5612. (b) Field, M. J.; Bash, P. A.; Karplus, M. *J. Comput. Chem*. **1990**, *11*, 700. (c) Maseras, F.; Morokuma, K. *J. Comput. Chem*. **1995**, *16*, 1170. (d) Matsubara, T.; Maseras, F.; Koga, N.; Morokuma, K. *J. Phys. Chem*. **1996**, *100*, 2573. (e) Gao, J. In *Reviews in Computational Chemistry*; Lipkowitza, K. B., Boyd, D. B., Eds. VCH: New York, 1996; Vol. 7, p 119. (f) Sighn, J.; Kollman, P. A. *J. Comput. Chem*. **1996**, *7*, 718. (g) Troung, T. N.; Troung, T. T.; Stefanovich, E. V. *J. Chem. Phys.* **1997**, *107*, 1881. (h). Bakowies, D.; Thiel, W. *J. Phys. Chem*. **1996**, *100*, 10580.

(33) Cui, Q.; Karplus, M. *J. Chem. Phys*. **2000**, *112*, 1133.

(34) Frisch, M. J.; Trucks, G. W.; Schlegel, H. B.; Scuseria, G. E.; Robb, M. A.; Cheeseman, J. R.; Zakrzewski, V. G.; Montgomery, J. A., Jr.; Stratmann, R. E.; Burant, J. C.; Dapprich, S.; Millam, J. M.; Daniels, A. D.; Kudin, K. N.; Strain, M. C.; Farkas, O.; Tomasi, J.; Barone, V.; Cossi, M.; Cammi, R.; Mennucci, B.; Pomelli, C.; Adamo, C.; Clifford, S.; Ochterski, J.; Petersson, G. A.; Ayala, P. Y.; Cui, Q.; Morokuma, K.; Malick, D. K.; Rabuck, A. D.; Raghavachari, K.; Foresman, J. B.; Cioslowski, J.; Ortiz, J. V.; Stefanov, B. B.; Liu, G.; Liashenko, A.; Piskorz, P.; Komaromi, I.; Gomperts, R.; Martin, R. L.; Fox, D. J.; Keith, T.; Al-Laham, M. A.; Peng, C. Y.; Nanayakkara, A.; Gonzalez, C.; Challacombe, M.; Gill, P. M. W.; Johnson, B.; Chen, W.; Wong, M. W.; Andres, J. L.; Gonzalez, C.; Head-Gordon, M.; Replogle, E. S.; Pople, J. A. *Gaussian 98*, revision A.6; Gaussian, Inc.: Pittsburgh, PA, 1998.

(35) deDios, A. C.; Oldfield, E. *Chem. Phys. Lett.* **1993**, *205*, 108.

(36) (a) deDios, A. C.; Oldfield, E. *J. Am. Chem. Soc*. **1994**, *116*, 11485. (b) Pearson, J. G.; Le, H.; Sanders, L. K.; Godbout, N.; Halvin, R. H.; Oldfield, E. *J. Am. Chem. Soc*. **1997**, *119*, 11941.

(37) (a) Brüschweiler, R.; Case, D. A. *Prog. NMR Spectrosc*. **1994**, *26*, 27. (b) Scheurer, C.; Skrynnikov, N. R.; Lienin, S. F.; Straus, S. K.; Brüschweiler, R.; Ernst, R. R. *J. Am. Chem. Soc*. **1999**, *121*, 4242.

(38) Stefanovich, E. V.; Troung, T. N. *J. Phys. Chem. B* **1998**, *102*, 3018.

(39) Cremer, D.; Olsson, L.; Reichel, F.; Krake, E. *Isr. J. Chem.* **1993**, *33*, 369.

(40) Cammi, R.; Mennucci, B.; Tomasi, J. *J. Chem. Phys*. **1999**, *110*, 7627.

(41) Lienin, S. F.; Bremi, T.; Brutscher, B.; Brüschweiler, R.; Ernst, R. R. *J. Am. Chem. Soc*. **1998**, *120*, 9870.

(42) Lyne, P.; Hodoscek, M.; Karplus, M. *J. Phys. Chem*. **1999**, *103*, 3462.

(43) See, for example: Case, D. A. *Curr. Opin. Struct. Biol*. **1998**, *8*, 624.

(44) Pulay, P.; Wolinksi, K.; Hinton, J. F. *The Texas Program*; University of Arkansas: Fayetteville, AR, 1991.

(45) Salter, E. A.; Trucks, G. W.; Bartlett, R. J. *J. Chem. Phys*. **1989**, *90*, 1752.

(46) (a) Stone, A. J. *Chem. Phys. Lett*. **1981**, *83*, 233. (b) Stone, A. J.; Alderton, M. *Mol. Phys*. **1985**, *56*, 1047 (c) Stone, A. J. *The Theory of Intermolecular Forces*; Oxford University Press: Oxford, 1996.

(47) Svensson, M.; Humbel, S.; Froese, R. D.; Matsubara, T.; Sieber, S.; Morokuma, K. *J. Phys. Chem*. **1997**, *100*, 19357.

(48) Cui, Q.; Karplus, M. Work in progress.

(49) Day, P. N.; Jensen, J. H.; Gordon, M. S.; Webb, S. P.; Stevens, W. J.; Krauss, M.; Garmer, D.; Basch, H.; Cohen, D. *J. Chem. Phys*. **1996**, *105*, 1968.

(50) Haigh, C. W.; Mallion, R. B. *Prog. NMR Spectrosc*. **1980**, *13*, 303.

(51) (a) Ditchfield, R. *J. Chem. Phys*. **1976**, *65*, 3123. (b) Höller, R.; Lischka, H. *Chem. Phys. Lett*. **1981**, *84*, 94. (c) Chesnut, D. B.; Rusiloski, B. E. *J. Phys. Chem*. **1993**, *97*, 2839.

(52) (a) Becke, A. D. *Phys. Rev*. A **1988**, *38*, 3098. (b) Lee, C.; Yang, W.; Parr, R. G. *Phys. Rev. B* **1988**, *37*, 785. (c) Becke, A. D. *J. Chem. Phys*. **1993**, *98*, 5648.

(53) (a) Krishnan, R.; Binkley, J. S.; Seeger, R.; Pople, J. A. *J. Chem. Phys*. **1980**, *72*, 650.

(54) (a) Jorgensen, W. L.; Chandrasekhar, J.; Madura, J. P. *J. Chem. Phys*. **1983**, *79*, 926. (b) Neria, E.; Fisher, S.; Karplus, M. *J. Chem. Phys*. **1996**, *105*, 1902.

(55) Boys, S. F.; Bernardi, F. *Mol. Phys*. **1970**, *19*, 553.

(56) Ferchiou, S.; Giessner-Prettre, C. *Chem. Phys. Lett*. **1983**, *103*, 156.

(57) Flygare, W. H. *Chem. Rev*. **1974**, *74*, 653.

(58) Stillinger, F. H.; Rahman, A. *J. Chem. Phys*. **1974**, *60*, 1545.

(59) (a) Ditchfield, R.; Hehre, W. J.; Pople, J. A. *J. Chem. Phys*. **1971**, *54*, 724. (b) Hehre, W. J.; Ditchfield, R.; Pople, J. A. *J. Chem. Phys*. **1972**, *56*, 2257.

(60) MacKerell, A. D.; Wiorkiewiczkuczera, J.; Karplus, M. *J. Am. Chem. Soc*. **1995**, *117*, 11946.

(61) Kieft, J. S.; Tinoco, I., Jr. *Structure* **1997**, *5*, 713.

(62) Wedekind, J. E.; McKay, D. B. *Nat. Struct. Biol*. **1999**, *6*, 261.

(63) Markowski, V.; Sullivan, G. R.; Roberts, J. D. *J. Am. Chem. Soc*. **1977**, *99*, 714.

(64) See, for example: (a) no. 7 issue of *Chem. Rev*. **1996**, 96. (b) Fersht, A. *Structure and Mechanism in Protein Science*; W. H. Freeman and Company: New York, 1999.

(65) See, for example: (a) Saenger, W. *Principles of Nucleic Acid Structure*; Springer-Verlag: New York, 1984. (b) Draper, D. E.; Misra, V. K. *Nat. Struct. Biol*. **1998**, *5*, 927.

(66) (a) Vallee, B. L.; Auld, D. S. *Faraday Discuss*. **1992**, *93*, 47. (b) Vallee, B. L.; Auld, D. S. *Acc. Chem. Res*. **1993**, *26*, 543. (c) Vallee, B. L.; Auld, D. S. *Biochem*. **1993**, *32*, 6493.

(67) Klug, A.; Schwabe, J. W. R. *FASEB J*. **1995**, *9*, 597. (b) Berg, J. M.; Shi, Y. *Science* **1996**, *271*, 1081.

(68) (a) Eklund, H.; Nordstrom, B.; Zeppezauer, E.; Söderlund, G.; Ohlsson, I.; Boiwe, T.; Söderberg, B. O.; Tapia, O.; Brändén, C. I.; Åkeson, Å. *J. Mol. Biol*. **1976**, *102*, 27. (b) Eklund, E.; Samama, J. P.; Wallen, L.; Brändén, C. I.; Åkeson, Å.; Jones, T. A. *J. Mol. Biol*. **1981**, *146*, 561.

(69) Maret, W.; Larsen, K. S.; Vallee, B. L. *Proc. Nat. Acad. Sci*. *U.S.A.* **1997**, *94*, 2233.

(70) (a) Honzatko, R. B.; Crawford, J. L.; Monaco, H. L.; Ladner, J. E.; Edwards, B. F. P.; Evans, D. R.; Warren, S. G.; Wiley: D. C.; Ladner, R. C.; Lipscomb, W. N. *J. Mol. Biol*. **1982**, *160*, 219. (b) Lipscomb, W. N. *Adv. Enzymol*. *Relat. Areas Mol. Biol*. **1994**, *68*, 67.

(71) See, for example: (a) Cate, J. H.; Hanna, R. L.; Doudna, J. A. *Nat. Struct. Biol*. **1997**, *4*, 553. (b) Pyle, A. M. *Science* **1993**, *261*, 709.

(72) See, for example: (a) Kruger, K.; Grabowski, P. J.; Zaug, A. J.; Sands, J.; Gottschling, D. E.; Cech, T. R. *Cell* **1982**, *31*, 147. (b) Guerrier-Takada, C.; Gardiner, K.; Marsh, T.; Pace, N.; Altman, S. *Cell* **1983**, *35*, 849.

(73) (a) Pan, T.; Uhlenbeck, O. C. *Nature* **1992**, *358*, 560. (b) Pan, T.; Uhlenbeck, O. C. *Biochemistry* **1992**, *31*, 3887. (c) Legault, P.; Hoogstraten, C. G.; Metlitzky, E.; Pardi, A. *J. Mol. Biol*. **1998**, *284*, 325. (d) Hoogstraten, C. G.; Legault, P.; Pardi, A. R. *J. Mol. Biol*. **1998**, *284*, 337.

(74) (a) Kaupp, M.; Schleyer, P. v. R.; Stoll, H.; Preuss, H. *J. Chem. Phys* **1991**, *94*, 1360. (b) Kuechle, W.; Dolg, M.; Stoll, H.; Preuss, H. *Mol. Phys*. **1991**, *74*, 1245.

(75) (a) Hay, P. J.; Wadt, W. R. *J. Chem. Phys*. **1985**, *82*, 270; (b) **1985**, *82*, 284; (c) **1985**, *82*, 299.

(76) Allen, F. H.; Davies, J. E.; Galloy, J. J.; Johnson, O.; Kennard, O.; MacRae, C. F.; Mitchell, E. M.; Mitchell, G. F.; Smith, J. M.; Watson, D. G. *J. Chem. Inf. Comput. Sci*. **1991**, *31*, 187.

(77) McMahon, M. T.; deDios, A. C.; Godbout, N.; Salzmann, R.; Laws, D. D.; Le, H.; Havlin, R. H.; Oldfield, E. *J. Am. Chem. Soc*. **1998**, *120*, 4784.

(78) MacKerell, A. et al. *J. Phys. Chem*. B **1998**, *102*, 3586.

(79) Schafer, A.; Horn, H.; Ahlrichs, R. *J. Chem. Phys*. **1992**, *97*, 2571.

(80) Kachalova, G. S.; Popov, A. N.; Bartunik, H. D. *Science* **1999**, *284*, 473.

(81) (a) Augspurger, J. D.; Dykstra, C. E.; Oldfield, E. *J. Am. Chem. Soc*. **1991**, *113*, 2446. (b) Oldfield, E.; Guo, K.; Augspurger, J. D.; Dykstra, C. E. *J. Am. Chem. Soc*. **1991**, *113*, 7537.

(82) Kollwitz, M.; Gauss, J. *Chem. Phys. Lett*. **1996**, *260*, 639.

(83) Oppenheimer, N. J.; Davidson, R. M. *Org. Magn. Reson*. **1980**, *13*, 14.

(84) Cho, H.; Ramaswamy, S.; Plapp, B. V. *Biochemistry* **1997**, *36*, 382.

(85) Dejaegere, A. P.; Case, D. A. *J. Phys. Chem*. *A* **1998**, *102*, 5280.

(86) Mikkelsen, K. V.; Ruud, K.; Helgaker, T. *Chem. Phys. Lett*. **1996**, *253*, 443.

(87) (a) Malkin, V. G.; Malkina, O. L.; Steinebrunner, G.; Huber, H. *Chem.—Eur. J*. **1996**, *2*, 452. (b) Chesnut, D. B.; Rusiloski, B. E. *Chem. Phys. Lett*. **1994**, *314*, 19.

(88) Bopp, P.; Jancsò, G.; Heinzinger, K. *Chem. Phys. Lett*. **1983**, *98*, 129.

(89) (a) Nymand, T. M.; Åstrand, P.; Mikkelsen, K. *J. Phys. Chem*. **1997**, *101*, 4105. (b) Nymand, T. M.; Åstrand, P. *J. Chem. Phys*. **1997**, *106*, 8332.

(90) Brooks, C. L., III; Karplus, M. *J. Chem. Phys*. **1983**, *79*, 6312.

(91) Dang, L. X.; Pettitt, B. M. *J. Phys. Chem*. **1987**, *91*, 3349.

(92) Gao, J. *J. Chem. Phys*. **1998**, *109*, 2346.

(93) Soper, A. K.; Phillips, M. G. *Chem. Phys*. **1986**, *107*, 47.

(94) Lie, G. C.; Clementi, E. *Phys. Rev. A* **1986**, *33*, 2679.

(95) (a) Hindman, J. C. *J. Chem. Phys*. **1966**, *44*, 4582. (b) Raynes, W. T. *Nucl. Magn. Resn*. **1978**, *7*, 1. (c) Florin, A. E.; Alei, M. *J. Phys. Chem*. **1967**, *47*, 4268. (d) Raynes, W. T. *Mol. Phys*. **1983**, *49*, 443.